Global and Planetary Change 160 (2018) 123–142

Contents lists available at ScienceDirect

Global and Planetary Change

journal homepage: www.elsevier.com/locate/gloplacha

The distribution and hydrological significance of rock glaciers in the Nepalese Himalaya

D.B. Jones[a,*], S. Harrison[a], K. Anderson[b], H.L. Selley[a], J.L. Wood[e], R.A. Betts[c,d]

[a] College of Life and Environmental Sciences, University of Exeter, Penryn Campus, Penryn, Cornwall TR10 9EZ, UK
[b] Environment and Sustainability Institute, University of Exeter, Penryn Campus, Penryn, Cornwall TR10 9EZ, UK
[c] College of Life and Environmental Sciences, University of Exeter, Streatham Campus, Exeter EX4 4QE, UK
[d] Met Office, FitzRoy Road, Exeter, Devon EX1 3PB, UK
[e] Department of Geography, King's College London, Strand, London, WC2R 2LS

ARTICLE INFO

Editor: Dr. Sierd Cloetingh

Keywords:
Nepalese Himalaya
Nepal
Rock glacier
Inventory
Water equivalent
Geomorphological mapping

ABSTRACT

In the Nepalese Himalaya, there is little information on the number, spatial distribution and morphometric characteristics of rock glaciers, and this information is required if their hydrological contribution is to be understood. Based on freely available fine spatial resolution satellite data accessible through Google Earth, we produced the first comprehensive Nepalese rock glacier inventory, supported through statistical validation and field survey. The inventory includes the location of over 6000 rock glaciers, with a mean specific density of 3.4%. This corresponds to an areal coverage of 1371 km^2. Our approach subsampled approximately 20% of the total identified rock glacier inventory (n = 1137) and digitised their outlines so that quantitative/qualitative landform attributes could be extracted. Intact landforms (containing ice) accounted for 68% of the subsample, and the remaining were classified as relict (not containing ice). The majority (56%) were found to have a northerly aspect (NE, N, and NW), and landforms situated within north- to west-aspects reside at lower elevations than those with south- to- east aspects. In Nepal, we show that rock glaciers are situated between 3225 and 5675 m a.s.l., with the mean minimum elevation at the front estimated to be 4977 ± 280 m a.s.l. for intact landforms and 4541 ± 346 m a.s.l. for relict landforms. The hydrological significance of rock glaciers in Nepal was then established by statistically upscaling the results from the subsample to estimate that these cryospheric reserves store between 16.72 and 25.08 billion m^3 of water. This study, for the first time, estimates rock glacier water volume equivalents and evaluates their relative hydrological importance in comparison to ice glaciers. Across the Nepalese Himalaya, rock glacier to ice glacier water volume equivalent is 1:9, and generally increases westwards (e.g., ratio = 1:3, West region). This inventory represents a preliminary step for understanding the spatial distribution and the geomorphic conditions necessary for rock glacier formation in the Himalaya. With continued climatically-driven ice glacier recession, the relative importance of rock glaciers in the Nepalese Himalaya will potentially increase.

1. Introduction

The Hindu Kush-Himalayan (HKH) region contains ~54,000 glaciers covering an area of ~60,000 km^2 (Bajracharya and Shrestha, 2011), constituting the most extensive glacier coverage outside of the polar regions and forming the "Asian water towers" (Immerzeel et al., 2010). HKH-derived glacier and snowpack meltwater is important in sustaining seasonal water availability, and the food- and water-security of millions (Viviroli et al., 2007; Immerzeel et al., 2010; Kohler et al., 2014). HKH glaciers have generally undergone mass loss between 1980 and 2010 (Bajracharya et al., 2015), with estimated glacial mass change rates of −26 ± 12 Gt year^{-1} (2003–2009) (Gardner et al., 2013), while substantial further long-term glacial mass losses are projected under climate warming (Bolch et al., 2012; Jiménez Cisneros et al., 2014; Huss and Hock, 2015; Shrestha et al., 2015). The recession and, in some locations, loss of high-altitude frozen water stores may have significant consequences for downstream water supply (Immerzeel et al., 2010; Bolch et al., 2012), particularly following peak non-renewable water (Gleick and Palaniappan, 2010), with long-term decreased summer runoff projected (e.g., Sorg et al., 2014a; Sorg et al., 2014b). However, more climatically resilient permafrost features, including intact rock glaciers, contain ground ice volumes of potentially

* Corresponding author.
E-mail addresses: dj281@exeter.ac.uk (D.B. Jones), Stephan.Harrison@exeter.ac.uk (S. Harrison), Karen.Anderson@exeter.ac.uk (K. Anderson), joanne.wood@kcl.ac.uk (J.L. Wood), R.A.Betts@exeter.ac.uk (R.A. Betts).

https://doi.org/10.1016/j.gloplacha.2017.11.005
Received 1 August 2017; Received in revised form 11 October 2017; Accepted 3 November 2017
Available online 08 November 2017

significant hydrological value (e.g., Rangecroft et al., 2015).

Rock glaciers are cryospheric landforms formed by gravity-driven creep of ice-supersaturated accumulations of rock debris, incorporating a perennially frozen mixture of poorly sorted angular-rock debris and ground ice (Haeberli et al., 2006). They are characterised by a seasonally frozen, clastic blocky surficial layer 0.5 to 5 m thick that thaws each summer (known as the *active layer*) (Bonnaventure and Lamoureux, 2013; Pourrier et al., 2014). Critically, compared to clean-ice glaciers, the active layer has been shown to slow melt of ground ice within rock glaciers (Humlum, 1997; Bonnaventure and Lamoureux, 2013; Gruber et al., 2016). Rock glaciers thus potentially form key hydrological stores in semi- and arid-mountains, e.g., dry Andes, South America (Brenning, 2005b; Azócar and Brenning, 2010; Rangecroft et al., 2014), and are expected to form a larger component of base flow to rivers/streams under climate warming (Janke et al., 2015).

There have been a great number of inventories compiled for rock glacier distribution in various mountain ranges, for instance in central Europe (Chueca, 1992; Imhof, 1996; Guglielmin and Smiraglia, 1997; Baroni et al., 2004; Nyenhuis et al., 2005; Roer and Nyenhuis, 2007; Cremonese et al., 2011; Krainer and Ribis, 2012; Seppi et al., 2012; Bodin, 2013; Scotti et al., 2013; Colucci et al., 2016; Salvador-Franch et al., 2016; Triglav-Čekada et al., 2016; Winkler et al., 2016a; Onaca et al., 2017), Greenland and Scandinavia (Sollid and Sørbel, 1992; Humlum, 2000; Lilleøren and Etzelüller, 2011), Iceland (Etzelmüller et al., 2007), North America (Ellis and Calkin, 1979; Janke, 2007; Johnson et al., 2007; Millar and Westfall, 2008; Page, 2009; Liu et al., 2013; Charbonneau, 2015; Legg, 2016), South America (Brenning, 2005b; Perucca and Esper Angillieri, 2008; Esper Angillieri, 2009; Azócar and Brenning, 2010; Perucca and Esper Angillieri, 2011; Falaschi et al., 2014; Rangecroft et al., 2014; Falaschi et al., 2015; Azócar et al., 2016; Falaschi et al., 2016; Janke et al., 2017), Asia (Gorbunov et al., 1998; Ishikawa et al., 2001; Bolch and Marchenko, 2006; Regmi, 2008; Bolch and Gorbunov, 2014; Schmid et al., 2015; Wang et al., 2016) and New Zealand (Brazier et al., 1998; Allen et al., 2008; Sattler et al., 2016). However, rock glaciers in the HKH are comparatively less well studied, particularly within the Nepalese Himalaya where no inventory exists. Additionally, previous studies that have been carried out in the HKH were conducted at localised extents or are incomplete (e.g., Gorbunov et al., 1992; Jakob, 1992; Barsch and Jakob, 1998; Gorbunov et al., 1998; Owen and England, 1998; Shroder et al., 2000; Ishikawa et al., 2001; Regmi, 2008; Bolch and Gorbunov, 2014; Schmid et al., 2015). Thus, the hydrological contribution of these 'hidden ice' features to streamflow in the HKH is completely unknown. A full understanding of all inputs to the high-altitude hydrological cycle, including rock glaciers, is necessary for effective water resource management to mitigate or adapt to the impacts of climate change, particularly given that the HKH supplies water to millions of people.

In this context, the primary objectives of this study were to map the distribution of rock glaciers across the Nepal Himalaya (Fig. 1) and assess their hydrological significance, compared to glaciers, at regional and national spatial scales. The genesis of rock glaciers remains contested; this controversy has been between the *permafrost school* (purely periglacial-origin) vs. the *continuum school* (glacial- and periglacial-origin), and has previously been summarised and discussed in detail (see Berthling, 2011). Discussion of this is beyond the scope of this study; therefore, here we adopt the inclusive, and non-genetic, terms *discrete debris accumulations* (herein DDAs) and *ice-debris landforms* (herein I-DLs) to incorporate rock glaciers, protalus lobes and protalus ramparts. Ground ice is present within I-DLs (Harrison et al., 2008; Jarman et al., 2013).

2. Regional setting

Located within the HKH region, Nepal is situated between 26°22′ to 30°27′N latitude and 80°04′ to 88°12′E longitude extending ~800 km east to west and an average ~140 km north to south (Fig. 1). Nepal encompasses an area of 147,181 km^2, divided into five principal physiographical regions: Terai Plain, Siwalik Hills, Middle mountains, High mountains (inclusive of the Main Himalayas and the Inner Himalayan valleys), and the High Himalaya (see Shrestha and Aryal, 2011). In this study, our work was primarily concerned with the High Himalaya as this is where the majority of the permafrost region is found. Encompassing the area ≥ 4000 m a.s.l. (metres above sea level), this region is characterised by extremely rugged terrain and is home to eight of the ten highest peaks in the world including Mount Everest (8848 m a.s.l.). Furthermore, ~3800 glaciers covering ~3900 km^2 (~3%) of the total area of Nepal are primarily situated within this physiographic region (Bajracharya and Shrestha, 2011). The snowline altitude is ~5000 m a.s.l. (Shrestha and Joshi, 2011) with ~14,200 km^2 (~10%) of the total area of Nepal located above this elevation.

Due to the topographical extremes of the High mountains and High Himalaya, the climate type ranges from subtropical in the south to arctic in the north. The Asian summer monsoon dominates the climate of Nepal, providing most of the precipitation during June–September (Shrestha and Aryal, 2011); dependent on the location, ~80% of annual precipitation may occur within this period (Shrestha, 2000). Winter and spring precipitation predominantly falls as snow, forming snowpack stores that provide critical meltwater during the dry season (February–April). Alongside snowpack melt, glacier-derived meltwater contributions are important for maintaining perennial flow of the major rivers in Nepal and also the Ganges in India (Shrestha and Aryal, 2011). Consequently, projected reductions in glacial coverage under climate change, compounded by poor infrastructure and high population growth (Udmale et al., 2016), will have regional consequences for water resource availability (Shrestha and Aryal, 2011).

3. Materials and methods

3.1. Compilation of the DDA/I-DL inventory

Whereas automated and semi-automated techniques have enabled mapping and monitoring of clean-ice glaciers from optical satellite image data (e.g., Bolch and Kamp, 2006; Bhambri and Bolch, 2009; Shukla et al., 2010), these approaches are generally unsuitable for mapping debris-covered glaciers (e.g., Alifu et al., 2015) and rock glaciers (e.g., Brenning, 2009). This is because both supraglacial-debris (upon the glacier) and debris along the glacier margins originate from surrounding valley rock, thus spectral similarity of features "render[s] them mutually indistinguishable" (Shukla et al., 2010; Shukla and Ali, 2016). Therefore, following the methodology used in other inventory studies (e.g., Baroni et al., 2004; Scotti et al., 2013; Falaschi et al., 2014; Rangecroft et al., 2014) manual feature identification and digitisation using geomorphic indicators was the optimal approach for DDA/I-DL inventory compilation.

3.1.1. Remote sensing data

The inventory was generated using expert photomorphic mapping from fine spatial satellite image data (5–30 m resolution) accessible freely through Google Earth (version 7.1.5.1557, Google Inc., California, USA), including SPOT and DigitalGlobe (e.g., QuickBird, Worldview-1 and 2 and IKONOS) (Schmid et al., 2015). Google Earth has been used previously as a platform for mapping in a wide range of research areas (see Yu and Gong, 2012), and is particularly useful for large-scale geomorphological surveys (e.g., Bishop et al., 2014; Rangecroft et al., 2014; Schmid et al., 2015). Additionally, Google Earth Pro incorporates user-friendly GIS tools, enabling the creation of user-defined databases exportable as KML formatted files for further spatial analysis in a GIS environment (e.g., ArcGIS©) or data dissemination (e.g., Cremonese et al., 2011; Liu et al., 2013; Schmid et al., 2015). In this study, inventory data are shared as an open-source geodatabase (see Supplementary Information), and we argue that data dissemination through KML formatted files for use with free platforms

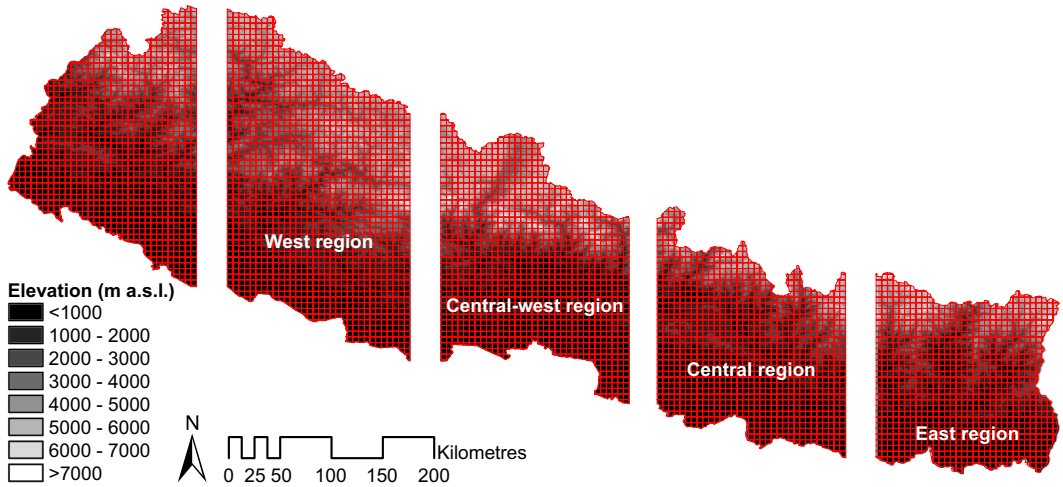

Fig. 1. Overview map of Nepal, including the gridded overlay, overlaid on a 30 m SRTM DEM. Five geographic sectors were defined and subsequently used in this research: the Far-west region, West region, Central-west region, Central region and the East region.

such as Google Earth is a positive step towards scientific transparency and open-access research. This has advantages for both the scientific and local/regional communities.

Topographic data were derived from a ~30 m resolution digital elevation model (DEM) created from the NASA Version 3.0 Shuttle Radar Topography Mission (SRTM) Global 1 arc-second data (herein referred to as "SRTM30") (for further information see USGS, 2015). Freely available SRTM30 data permits topographic analysis of DDAs/I-DLs, where finer resolution products (e.g., WorldDEM™ [~12 m], AW3GTM [~5 m]) are prohibitively expensive (Watson et al., 2015). STRM DEMs have been successfully used in previous inventory studies in mountain regions (e.g., Bolch and Gorbunov, 2014; Schmid et al., 2015).

3.1.2. Landform digitisation and database composition

DDAs and I-DLs were identified and 'pinned' within Google Earth Pro according to the presence of geomorphic indicators (Table 1). This resulted in an initial point-based inventory for Nepal. The pinning methodology relied on using a gridded search methodology to ensure that the digitisation was exhaustive. To create the grid, in ArcGIS, the study region was divided using a vector overlay of ~25 km^2 grid squares (Fig. 1). Subsequently the gridded overlay was imported into Google Earth Pro and each grid square was visually surveyed on an individual basis. The study region was split into five geographic sectors of equal longitudinal-width, loosely adapted from the Nepalese Administrative Districts: (i) East region (86°34′–88°12′E); (ii) Central region (84°56′–86°34′E); (iii) Central-west region (83°18′–84°56′E); (iv) West region (81°40′–83°18′E); and (v) Far-west region (80°02′–81°40′E) (Fig. 1).

From the point-based inventory, a ~20% sample of the identified DDAs/I-DLs from each region were randomly selected using ArcGIS (version 10.3.1, ESRI, Redlands, CA, USA) and their geographic boundaries digitised within Google Earth Pro, forming a polygonised-inventory within which more detailed spatial attributes were measured. The pseudo-3D viewer in Google Earth provided topographic context for landforms, and hence aided delineation of DDA/I-DL boundaries. Furthermore, the availability of multi-temporal satellite image data within Google Earth was critical for reducing the mapping uncertainty associated with poor quality image data (affected by, for instance, clouds, snow cover, and long cast shadows on steep-north facing slopes). This enabled the generation of a more complete inventory.

The methodology of Scotti et al. (2013) was adopted for DDA/I-DL boundary digitisation. The outline of the entire landform surface, from the rooting zone to the base of the front slope (Barsch, 1996), was digitised for each of the randomly sampled subset of DDAs/I-DLs. Some aspects of digitisation were challenging: delimitation of the upper boundary of DDAs/I-DLs through geomorphic mapping, is arbitrary (Krainer and Ribis, 2012); determining the upper boundary of I-DLs lacking prominent landforms (e.g., furrow-and-ridge topography) within the rooting zone, particularly in the absence of knowledge regarding landform kinematics (i.e. movement), is difficult (e.g., Roer and Nyenhuis, 2007); and delineation of individual polygons where multiple DDAs/I-DLs coalesce into a single body, is inherently subjective (e.g., Scotti et al., 2013; Schmid et al., 2015). Within this study, "when the frontal lobes of two (or more) rock glaciers originating from distinct source basins join downslope, we consider the two components as separate bodies. Where the limits between lobes are unclear and the lobes share other morphological characteristics (e.g., degree of activity and vegetation cover), we classify the whole system as a unique rock glacier" (Scotti et al., 2013). Regarding cases where DDAs/I-DLs grade into

Table 1
Geomorphic indicators used for the identification of DDAs/I-DLs and their activity.

Geomorphic Indicator	Active	Relict
Surface flow structure	• Defined furrow-and-ridge topography (Kääb and Weber, 2004)	• Less defined furrow-and-ridge topography (Kääb and Weber, 2004)
Rock glacier body	• Swollen body (Baroni et al., 2004) • Surface ice exposures (e.g., Potter et al., 1998)	• Flattened body (Baroni et al., 2004) • Surface collapse features (Barsch and King 1975 in Janke et al., 2013)
Front slope	• Steep (~ > 30–35°) (Baroni et al., 2004) • Sharp crested frontal slope (Wahrhaftig and Cox, 1959) • Light-coloured (little clast weathering) frontal zone and darker varnished upper surface (e.g., Bishop et al., 2014)	• Gently sloping (~ < 30°) (Baroni et al., 2004) • Gentle transition (rounded crest) to upper surface (Wahrhaftig and Cox, 1959)

Table 2
Inventory structure: attributes derived during DDA/I-DL mapping, with attribute explanation. See also Fig. 2.

Attribute	Attribute explanation
Name	[Region No.]Grid ID_Feature No._MMDDYYYY (NB: MMDDYYYY refers to satellite image date)
Region	[1] East [2] Central [3] Central-west [4] West [5] Far-west
DMSLon	Longitudinal coordinate of polygon centroid (DDD°MM′SS.sss [N|S])
DMSLat	Latitudinal coordinate of polygon centroid (DDD°MM′SS.sss [W|E])
MEF (m a.s.l.)	Minimum elevation at the front
MaxE (m a.s.l.)	Maximum elevation of the feature
Elevation_ (m a.s.l.)	Range|mean
Area (km^2)	/
Slope_ (°)	Maximum|minimum|range|mean
Mean_Aspect (°)	0–359
Aspect_Class	N, NE, E, SE, S, SW, W, NW (e.g., 90° = E, 180° = S)
Max_Length (m)	/
Max_Width (m)	/
Mean_Width (m)	/
L:W_Ratio	Length: width ratio
Geometry_Type	Shape: Tongue-shaped, lobate-shaped
Dynamic_Type	Active, Inactive, Relict
WVEQ_ (km^3)	Water volume equivalent: 40%|50%|60%
Upslope_Boundary	Glacier, slope
Index_Code	See Table 3
Certainty_Index	Medium_Certainty, High_Certainty, Virtual_Certainty

upslope landforms (e.g., a debris rock glacier is gradually developing form a terminal/lateral moraine), "a clear distinction between the two landforms cannot be set and we delineated the whole body (i.e., moraine plus rock glacier)" (Scotti et al., 2013). Both quantitative and qualitative landform attributes were extracted and recorded for each digitised DDA/I-DL (Table 2; Fig. 2). Within ArcGIS a regional projected coordinate system, Nepal Nagarkot TM, was used for attribute extraction and DDA/I-DL polygons were re-projected into the WGS84 coordinate system for exportation to KML formatted files. The quantitative data (i.e. area, length, width) were directly calculated in ArcGIS. Lengths (parallel to flow) were manually digitised within Google Earth Pro for each landform. Based on the methodology described by Frauenfelder et al. (2003), within ArcGIS widths (perpendicular to length) were digitised at ~50 m intervals, and mean width calculated in order to incorporate considerable width variation along the DDA/I-DL (Fig. 2). Additionally, landforms were classified into *tongue-shaped* or *lobate-shaped*, where the length: width ratio is > 1 or < 1 respectfully (Guglielmin and Smiraglia, 1998; Harrison et al., 2008).

Using ArcGIS surface raster functions, elevation, slope and aspect were calculated for the SRTM30 DEM. ArcGIS zonal statistics were used to overlay the polygonised DDAs/I-DLs onto SRTM30-derived raster surfaces to calculate minimum, maximum, range and mean elevation and slope for each landform. The minimum elevation at the front (MEF) for each DDA/I-DL was defined as the elevation at which the base of the

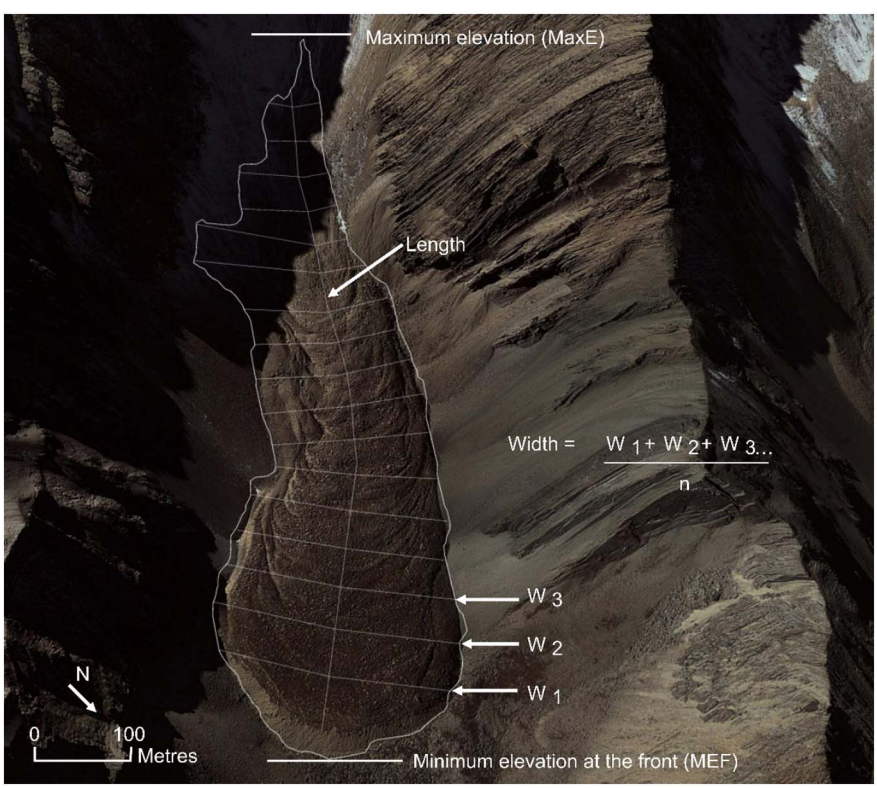

Fig. 2. Annotated diagram of landform attributes on DDA/I-DL (feature ID: [4]NEP1257_1_11052011), Nepal (29°06′20.36″N, 83°06′57.39″E). Image data: Google Earth, DigitalGlobe; imagery date: 05 November 2011.

front slope meets the slope downstream; the maximum elevation of the feature (MaxE) as the upper boundary (Scotti et al., 2013). As a circular parameter, mean aspect cannot be calculated using simple zonal statistics (i.e. the mean of 0° and 359° cannot be 180° [Davis 1986 in Janke, 2013]). The vector mean aspect ($\bar{\theta}$) was calculated in R (version 3.1.2, R Core Team, Vienna, Austria) using Eq. (1):

$$S = \sum \sin\theta, \quad C = \sum \cos\theta \qquad \bar{\theta} = \arctan\frac{S}{C} \tag{1}$$

where S is the sum of sine values of aspect (θ) (based on individual pixels of the surface rasters), and C is the sum of cosine values of aspect (Paul et al., 2009; Janke, 2013). The mean aspect was then recoded into 8 classes (N, NE, E, SE, S, SW, W, NW).

The degree of activity was determined considering the presumed ice content and movement of DDAs/I-DLs, in accordance with the morphological classification by Barsch (1996), using morphological- and geomorphological- criteria from satellite image interpretation. In our inventory, DDAs were categorised as *relict* (not containing ice, sometimes referred to as *fossil*) and I-DLs as *intact* (containing ice) (Table 1) (e.g., Cremonese et al., 2011; Scotti et al., 2013; Rangecroft et al., 2014; Onaca et al., 2017). The "intact" classification includes both *active* and *inactive* landforms.

Active landforms (I-DLs) are generally characterised by: distinctive surface micro-relief of furrow-and-ridge topography, predominantly the result of longitudinal compression (see Springman et al., 2012), gravity-driven viscous buckle folding (see Frehner et al., 2015) and/or the debris grain-size; steep lateral slopes; and steep frontal slopes near the angle of repose (Haeberli et al., 2006), all of which indicate ice presence (Barsch, 1996; Baroni et al., 2004). Inactive I-DLs also contain ice, but are immobile. Barsch (1996) suggest two possibilities that may account for this inactivity: (i) melting of the upper layers within the frontal slope, such that "the unfrozen mantle at the top of the front slope is more than 10 m thick" (Barsch, 1973 as cited in Barsch, 1996). This type of I-DL inactivity is called *climatic inactive*; or (ii) I-DLs "extend so far from their source area that the tangential stress due to the slope, the thickness of the deposit [e.g., insufficient talus-nourishment rates to feature rooting zones (e.g., Kellerer-Pirklbauer and Rieckh, 2016)], its bulk density etc. decrease below the limit required for movement" (Barsch, 1996). This type of I-DL inactivity is called *dynamic inactive*. Relict landforms (DDAs), "formerly active landforms in which ice is vanished" (Scotti et al., 2013), are characterised by: surface collapse features (Barsch and King 1975 in Janke et al., 2013); subdued surface micro-relief; less steep front- and lateral-slope(s) (Barsch, 1996; Baroni et al., 2004), resulting from permafrost degradation; and often extensive vegetation cover (Scotti et al., 2013).

Finally, in order to account for subjectivity associated with the identification, digitisation and classification of landforms in the inventory, we detailed the degree of 'uncertainty' through the application of a *Certainty Index score*, adapted from Schmid et al. (2015), for each digitised DDA/I-DL (Table 3). Uncertainties in the definition of: (i) external boundaries (i.e. outline); (ii) snow coverage; (iii) longitudinal flow structure; (iv) transverse flow structure; and (v) frontal slope were all recorded. Critically, this approach enables more complete mapping of DDAs/I-DLs despite occasionally poor satellite image data quality; for example, Schmid et al. (2015) sampled 4000 ∗ ~30 km^2 grids in the HKH region, of which ~410 samples (~12,300 km^2) were classified as insufficient quality (IQ), where IQ was defined as "poor image quality, excessive snow or cloud coverage *over any part of the sample*" and disregarded. Within this study, partially IQ grids are not disregarded, thus previously unidentified DDAs/I-DLs are mapped within this inventory.

3.2. Estimating hydrological stores

3.2.1. Ice-debris landforms

Estimations of I-DL water content (water volume equivalent [km^3]) were calculated based on presumed ice volumes stored within intact I-DLs (Brenning, 2005b; Azócar and Brenning, 2010; Rangecroft et al., 2015). I-DL ice volume content was estimated through multiplying estimated I-DL thickness and I-DL surface area and then by estimated ice content. Within this study, I-DL thickness and average ice content are unknown variables; direct measurements of I-DL internal structure within the HKH are limited, due to practicalities of field-based research (e.g., boreholes, geophysical investigations) in largely remote locations (Janke et al., 2013). Therefore, I-DL thickness was estimated through applying an empirical rule established by Brenning (2005a) (Eq. (2)), as applied in existing studies (e.g., Azócar and Brenning, 2010; Perucca and Esper Angillieri, 2011; Rangecroft et al., 2015; Janke et al., 2017); however, further research is needed to improve area-thickness relationships (Rangecroft et al., 2015).

$$\text{Mean I-DL thickness [m]} = 50 * (\text{I-DL area [km}^2\text{]})^{0.2} \tag{2}$$

By definition, I-DLs do not contain 100% ice. Ice content within I-DLs is spatially heterogenous, therefore estimating water volume equivalent is challenging due to difficulty in establishing I-DL genesis [i.e. periglacial origin and glacigenic origin] and subsequent ice depth and distribution (Seligman, 2009). Few geophysical investigations of I-DLs have been conducted within the HKH; those that have focus on quantifying ice presence, opposed to ice content by volume (e.g., Jakob, 1992; Ishikawa et al., 2001). Therefore, here estimated ice volume is 40–60% by volume (Barsch, 1996; Haeberli et al., 1998; Hausmann et al., 2012), enabling lower, average, and upper estimates to be calculated. Finally, water equivalent volume was calculated assuming an ice density conversion factor of 0.9 g cm^{-3} (≡ 900 kg m^{-3}) (Paterson, 1994).

3.2.2. Ice glaciers

Within this study, we set out to establish the relative contributions of rock glaciers and ice glaciers in the Nepalese Himalaya, therefore it was important to be able to compare quantitatively the estimated water equivalent volumes of rock glaciers vs. ice glaciers. Volume-area (V-A) scaling relations (e.g., Chen and Ohmura, 1990; Bahr et al., 1997), i.e. $V = cA^{\gamma}$ where glacier volume (V) is calculated as a function of surface area (A) and two scaling parameters (c and γ), are frequently used approaches for ice volume estimations (Frey et al., 2014). Indeed, V-A

Table 3
Certainty Index applied to each DDA/I-DL.

Parameter	Parameter options (index code)		
	1 point	2 points	3 points
External boundary	None (ON)	Vague (OV)	Clear (OC)
Snow coverage	Snow (SS)	Partial (SP)	None (SN)
Longitudinal flow structure	None (LN)	Vague (LV)	Clear (LC)
Transverse flow structure	None (TN)	Vague (TV)	Clear (TC)
Front slope	Unclear (FU)	Gentle (FG)	Steep (FS)
Certainty Index score	Medium certainty (MC) ≤ 5	High certainty (HC) 6 to 10	Virtual certainty (VC) ≥ 11

Table 4
Key mean characteristics for intact and relict landforms.

Region	Activity	No. of landforms	(%)	MEF (m a.s.l.)	MaxE (m a.s.l.)	Length (m)	Width (m)	Area (km^2)	Aspect	No. of landforms (upscaled)
East (86°34′–88°12′E)	Intact	93	58	4893	5076	569	232	0.16	Northwest	492
	Relict	66	42	4541	4705	413	200	0.10	Northwest	349
Central (84°56′–86°34′E)	Intact	22	36	4791	4997	549	220	0.14	North	128
	Relict	39	64	4480	4631	417	206	0.11	Northwest	226
Central-west	Intact	199	88	5141	5405	743	280	0.25	West	1081
(83°18′–84°56′E)	Relict	27	12	4409	4643	595	218	0.16	Northwest	147
West (81°40′–83°18′E)	Intact	347	64	4947	5192	829	272	0.29	West	1951
	Relict	191	36	4604	4800	557	230	0.16	North	1074
Far-west (80°02′–81°40′E)	Intact	111	73	4880	5109	807	262	0.27	Northeast	574
	Relict	42	27	4394	4666	662	228	0.18	Northwest	217
Total	Intact	772	68	4977	5215	765	266	0.25	West	4226
	Relict	365	32	4541	4738	531	221	0.15	Northwest	2013

MEF = minimum elevation at the front; MaxE = maximum elevation of landform.

relations have previously been used within rock glacier–ice glacier comparative studies (e.g., Azócar and Brenning, 2010; Perucca and Esper Angillieri, 2011; Rangecroft et al., 2015). However, V-A relations, and thickness-area scaling relations (see Frey et al., 2014), are designed to estimate the ice volumes of large-sample ensembles (> 20,000 minimum sample-limit [Cogley, 2011]); while suitable for global volumetric and/or thickness estimations (e.g., Huss and Farinotti, 2012; Marzeion et al., 2012; Grinsted, 2013), they are less so for smaller-samples or individual glaciers (Frey et al., 2014).

In the Himalayan-Karakoram region, Frey et al. (2014) report that V-A relations systematically overestimate ice volumes. Estimated ice volumes derived from the (Glacier bed Topography) ice-thickness distribution model (herein GlabTop2) (Frey et al., 2014), a new version of the GlabTop model (Linsbauer et al., 2009), are lower than results from V-A relations. Furthermore, direct comparison between GlabTop2 ice-thicknesses and local ice-thickness measurements derived from ground penetrating radar show good agreement; validation could not be undertaken for results from V-A relations (Frey et al., 2014). Therefore, here we use ice-thickness results for Nepal derived from GlabTop2 (Frey et al., 2014). The glacier outlines mapped by the International Centre for Integrated Mountain Development (Bajracharya and Shrestha, 2011) and the void-filled SRTM 3 arc-second data (~90 m resolution) were used for these calculations. Ice volumes were generated from the results following Eq. (3):

$$V = A * \sum H \tag{3}$$

where V represents ice volume, A the glacier surface area, and H the ice-thicknesses derived from GlabTop2. Subsequently, we calculated the water equivalent volume of ice glaciers, assuming 100% ice content by volume and applying the aforementioned ice density conversion factor.

3.3. Spatial and statistical inventory analysis

Here, statistical analysis was performed in R (bivariate statistics: one-way analysis of variance [ANOVA] and post hoc tests). One-way ANOVA and Tukey post hoc testing were used to investigate relationships and differences between independent qualitative variables (region, activity status, slope aspect class) and quantitative dependent variables (MEF, landform area, landform length) with the statistical significance evaluated at the $p \leq 0.05$ level. To satisfy the assumptions of ANOVA tests, i.e. normally distributed population, a logarithmic transformation was applied to landform area and length. ArcGIS and R were used to assess the relationship between landform slope aspect and hillslope aspect frequency for Nepalese mountain slopes.

4. Results

4.1. Inventory analysis

In total, 6239 DDAs/I-DLs were pinned across the Nepalese Himalaya. The upscaled estimates indicated that 4226 and 2013 landforms were classified as intact and relict respectively (Table 4; see Fig. A.1). Estimated total upscaled DDA/I-DL area is 1371 km^2, representing ~31% of the area covered by clean-ice glaciers in the same region (4426 km^2). Overall, 1137 landforms were digitised (Fig. 3; Table 4) and this detailed subsample covered a total surface area of 249.83 km^2. Most of these landforms, 772 (68%), were classified as intact, covering 196.52 km^2, while the remaining 365 (32%) covered 53.31 km^2, and were classified as relict. Ninety-one percent of DDAs/I-DLs were classified as tongue-shaped. Ninety percent of DDAs/I-DLs were situated between ~4200 and ~5400 m a.s.l., with the calculated mean MEF of intact landforms (herein I-DLs; 4977 ± 280 m a.s.l.) at a higher altitude than that of relict landforms (herein DDAs; 4541 ± 346 m a.s.l.) (Table 4). DDA/I-DL characteristics were analysed regionally and Nepal-wide. The open-source geodatabase within the Supplementary Information (Jones, 2017) provides detailed information for the subsampled DDAs/I-DLs. Additionally, the Nepal inventory KML file of both the pinned landforms (totalling 6239 DDAs/I-DLs) and the detailed subsample (totalling 1137 DDAs/I-DLs) are shared within the supplementary data.

4.1.1. Landform elevation and distribution

DDAs and I-DLs were situated within an elevation range of 3225 to 5675 m a.s.l. (Fig. 4). Nationally, the mean MEF for DDAs/I-DLs was 4837 ± 365 m a.s.l. (Table 4). Although remotely-based classification of DDAs/I-DLs has associated limitations, the histogram and boxplots of MEFs across regions provide indirect qualitative validation of inventory reliability. Specifically, reported mean MEFs demonstrate that I-DLs consistently occurred at higher elevations than DDAs (Figs. 4 and 5).

The majority of I-DLs identified are located above 4600 m a.s.l. (92%), with most situated within the 4800–5200 m a.s.l. (51%) elevation belt (Fig. 5). Relict landforms (DDAs) cluster predominantly between 4200 and 4800 m a.s.l. (62%), and 4400–4800 m a.s.l. (43%) in particular (Fig. 5). Nationally, the mean MEF for all I-DLs was 4977 ± 280 m a.s.l. (Table 4), ranging between 4110 and 5675 m a.s.l. The highest I-DL was located in the Central-west region at 5675 m a.s.l. ([3]NEP1186_1_10-25-2011). The mean MEF for all DDAs Nepal-wide was 436 m lower than that of I-DLs, at 4541 ± 346 m a.s.l. (Table 4), with a range of 3225 to 5482 m a.s.l. The highest DDA was situated in the West region at 5482 m a.s.l. ([4]NEP637_1_10-14-2010). I-DLs are located at statistically higher MEFs than DDAs at the national scale (ANOVA: F-value = 513.43, *df* within groups = 1, between groups = 1135, $p \leq 0.001$); Tukey post hoc testing showed I-DLs were

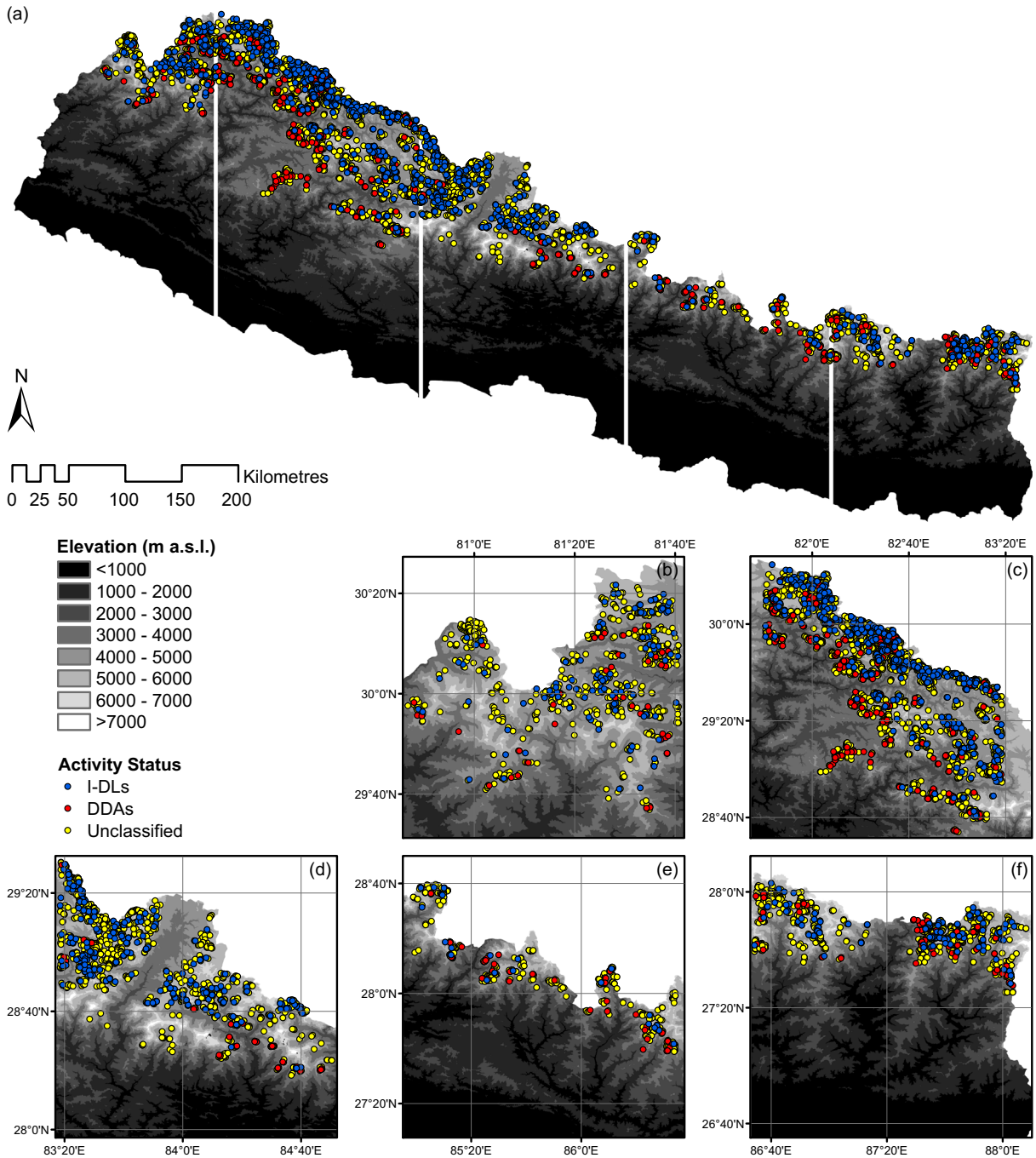

Fig. 3. Distribution of DDAs and I-DLs overlaid on a 30 m SRTM DEM for the: (a) entirety of Nepal; (b) Far-west region; (c) West region; (d) Central-west region; (e) Central region; and (f) East region. Landforms with unclassified activity status (i.e. pinned rock glaciers that were not digitised) are depicted for completeness.

situated at statistically higher MEFs than DDAs in all sub-regions, with the greatest difference seen in the Central-west region (Diff = 732, $p \leq 0.001$) and smallest in the Central region (Diff = 310, $p \leq 0.001$). Fig. 4 shows that the largest MEF elevation spread of I-DLs occurs within the West region (4110 to 5628 m a.s.l., range = 1518 m), while that of DDAs occurs within the Far-west region (3225 to 5090 m a.s.l., range = 1865 m). The Central region had the smallest elevation range of both I-DLs (4553 to 5137 m a.s.l., range = 584 m) and DDAs (3968 to 5118 m a.s.l., range = 1150 m).

The spatial distribution of DDAs/I-DLs among the five sub-regions is also somewhat inhomogeneous; total landform numbers vary from 354 (~6%) in the Central region to 3025 (~48%) in the West region (Table 4). Available suitable area, i.e. terrain ≥ 3225 m a.s.l., appears to be key to DDA/I-DL development and sustainability in the Nepalese Himalaya. Mountainous terrain ≥ 3225 m a.s.l. comprises ~43,500 km^2 (~27%) of Nepal. Those regions with the largest proportional area ≥ 3225 m a.s.l., correspondingly have the largest proportion of DDAs/I-DLs (Table 5). The overall mean density (n km^{-2}) of DDAs/I-DLs ranges between 0.09 (Central region) and 0.19 (West region), with an I-DL mean density of 0.10 and DDA mean density of 0.05 (Table 5). Considering the specific landform area ≥ 3225 m a.s.l., values are greatest in the West region (4.69 ha km^{-2}) followed by the Far-west region (3.69 ha km^{-2}) and tend to decrease eastwards, with specific landform areas below the mean value (3.40 ha km^{-2}) in all remaining regions (Table 5).

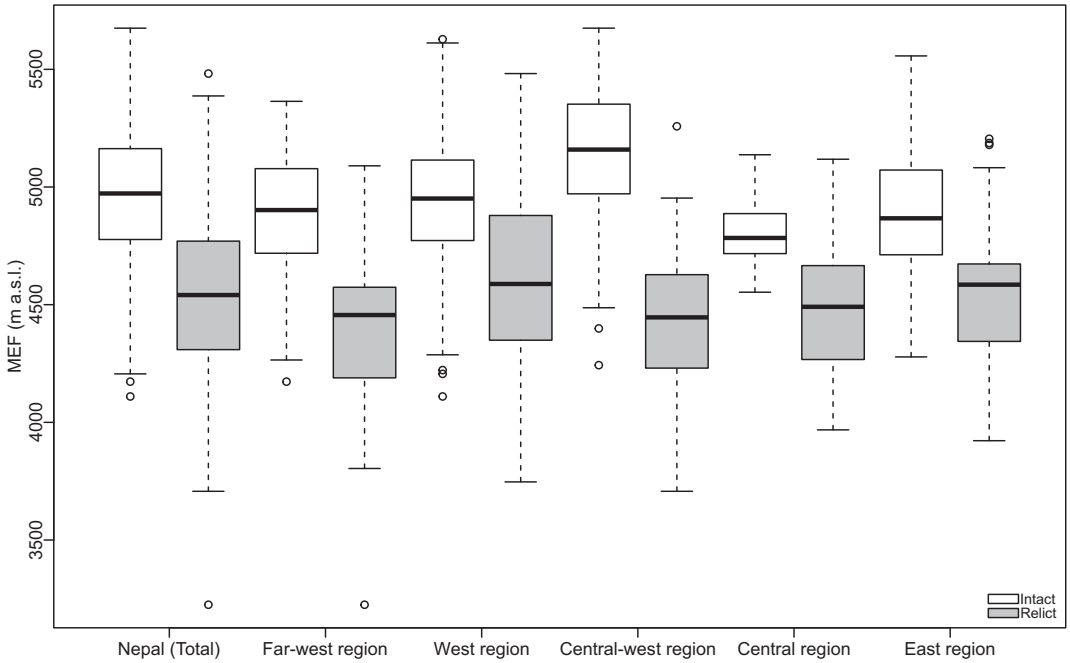

Fig. 4. Boxplot showing the distribution of DDA/I-DL minimum elevation at fronts (MEFs) Nepal-wide (Total) and regionally from west to east. Here, the whiskers extend to either the minimum and maximum of the data, or 1.5 times the interquartile range, whichever is smaller. The circles represent outliers.

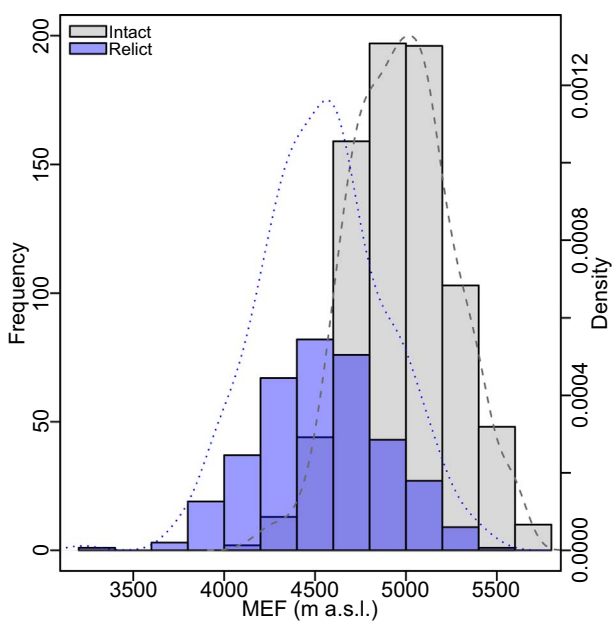

Fig. 5. Nepal-wide frequency analysis of intact and relict landform MEF, grouped into classes of 200 m of elevation. The fitted lines represent a normal (Gaussian) distribution.

4.1.2. Landform aspect

Generally, north-facing slopes dominate the development and formation of DDAs/I-DLs. Forty-four percent of landforms are situated within north-facing aspects (NW, 15%; NE, 15%; N, 14%), while 17% have developed on west-facing slopes. Furthermore, taken as a whole, the mean aspect suggests DDAs/I-DLs are predominantly situated on north-western ($\overline{X}$=314°) slopes.

Activity classification of observed landforms shows that I-DLs are more evenly distributed across aspect classes, while DDAs are predominantly situated on north- (56%: NW, 21%; N, 19%; NE, 16%) and west-facing (17%) slopes, with 5 to 9% located in each of the remaining aspect classes (Fig. 6a). I-DLs within the inventory show a mean aspect of 288°, with a circular variance of 0.13. Circular variance, defined as $CV = 1 - \overline{R}$ where the quantity $\overline{R}$ is the mean resultant length, indicates the dispersion of individual values around the mean, ranging between 0 and 1; values close to 1 suggest low dispersion (Davis, 2002: p. 321). DDAs show a mean aspect of 333°, with a circular variance of 0.34, therefore exhibit comparatively less dispersion than I-DLs. Regionally, with the exception of the Central-west region, a greater proportion (%) of I-DLs are situated within the northern- compared to the southern-quadrant (Table 6; Fig. 6b–f). DDAs within all regions are predominantly situated within the northern quadrant (48 to 69%) compared to the southern quadrant (13 to 29%) (Table 6; Fig. 6b–f).

Taken as a whole, landforms situated within the northern aspect quadrant occur at consistently lower elevations compared to DDAs/I-

Table 5
DDA/I-DL proportion, proportional area ≥ 3225 m a.s.l., DDA/I-DL density and DDA/I-DL specific area across the sub-regions of Nepal. Where appropriate, values are reported to two decimal places.

	East (86°34′–88°12′E)	Central (84°56′–86°34′E)	Central-west (83°18′–84°56′E)	West (81°40′–83°18′E)	Far-west (80°02′–81°40′E)
DDA/I-DL proportion	13%	6%	20%	48%	13%
Proportional area ≥ 3225 m a.s.l.	14%	10%	25%	39%	13%
Density (n km^{-2})[a]	0.15	0.09	0.12	0.19	0.15
Specific area (ha km^{-2})[b]	2.01	1.11	2.92	4.69	3.69

[a] Density (n km^{-2}) was calculated by considering the regional area ≥ 3225 m a.s.l. (MEF of lowest observed landform).
[b] Specific area (ha km^{-2}) where 'ha' reflects DDA/I-DL area, was also calculated by considering the regional area ≥ 3225 m a.s.l. The upscaled results were used within calculations of both density and specific area.

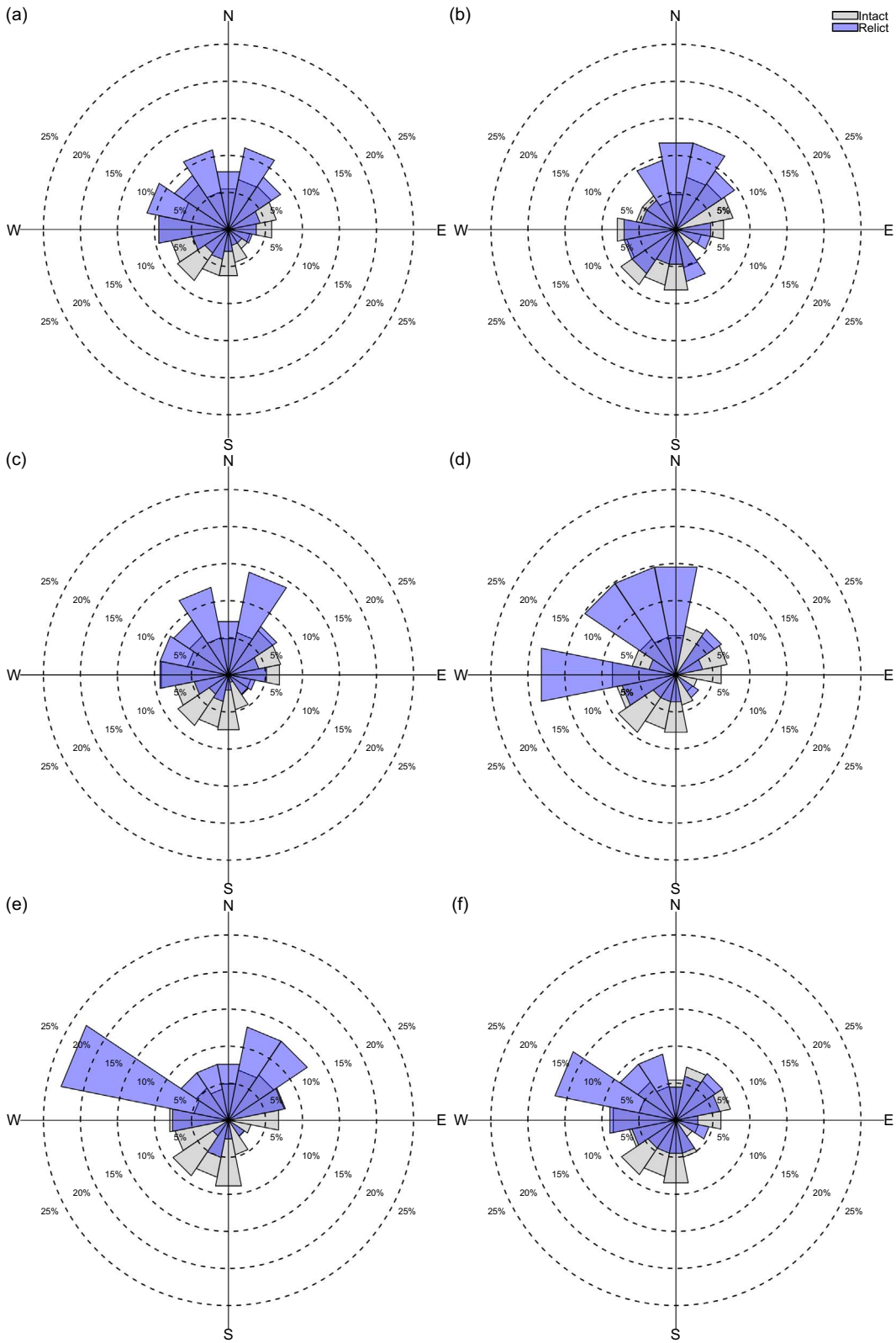

Fig. 6. Rose plots showing the relative abundance (%) of intact and relict landforms across slope aspects within: (a) Nepal-wide (Total); (b) Far-west region; (c) West region; (d) Central-west region; (e) Central region; and (f) East region. The angular interval is 22.5°.

DLs located within the southern aspect quadrant (Figs. 7, 8 and 9a). This altitudinal mismatch ranges between 25 m (Far-west region) to 307 m (West region) ($\overline{X}$=240 m), and is reflected within both I-DLs and DDAs at $\overline{X}$= 166 m and $\overline{X}$= 152 m, respectively. Regionally, with the exception of the Far-west region where both I-DLs ($\overline{X}$=5 m) and DDAs ($\overline{X}$=81 m) situated within the southern quadrant occur at lower elevations, all regions reflect this observation.

Nationally, ANOVA showed statistically significant differences between aspect class and DDA/I-DL MEF (F-value = 17.94, *df* within groups = 7, between groups = 1129, $p \leq 0.001$). Tukey post hoc

Table 6
Regional aspect classification of DDAs and I-DLs into north- (292.5 to 67.5°) and south- (112.5 to 247.5°) facing aspect quadrants.

Activity	Aspect quadrant	Region				
		East (86°34′–88°12′E)	Central (84°56′–86°34′E)	Central-west (83°18′–84°56′E)	West (81°40′–83°18′E)	Far-west (80°02′–81°40′E)
Intact	North (NW, N, NE)	41%	55%	33%	39%	45%
	South (SW, S, SE)	35%	23%	39%	32%	29%
Relict	North (NW, N, NE)	48%	69%	56%	57%	52%
	South (SW, S, SE)	24%	13%	22%	17%	29%

testing confirms that DDAs/I-DLs situated within the northern aspect quadrant and western slope aspects, occur at statistically lower MEFs than those found within the southern aspect quadrant and east slope aspects (Fig. 8).

Slope aspect appears to have little influence on landform size (Fig. 9b), and no significant difference was found (ANOVA: F-value = 0.79, *df* within groups = 7, between groups = 1097, $p = 0.597$). Both DDA and I-DL mean size is largest on east-facing slopes. Indeed, the largest I-DL encompassing 3.55 km^2 is located on a south-facing slope ([4]NEP74_2_12-22-2011). Slope aspect appears to affect areal distribution (Fig. 9c). DDA total area in the northern quadrant, ~30 km^2, is greater than that in the southern quadrant, ~10 km^2. In contrast, the pattern of I-DL total area is relatively homogenous across aspect classes, with two exceptions; the peak and trough in west and southeast aspect classes respectively (Fig. 9c). Fig. 10a demonstrates that the frequency of hillslope aspects ≥ 3225 m a.s.l. in the Nepalese Himalaya are relatively uniform, whereas Fig. 10b reaffirms the relative dominance of the northern and west aspect classes.

4.1.3. Landform morphology

The predominant geometry type (see Section 3.1.2) of landforms in the inventory was tongue-shaped (91%), a proportion reflected by both DDAs and I-DLs (91% and 90%, respectively). Landforms > 1 km in length form ~16% of the observed DDAs/I-DLs, examples of which are apparent in all five sub-regions. Remaining landforms were all < 1 km long; overall mean length was 690 ± 519 m, while I-DL and DDA mean length was calculated to be 765 ± 569 and 531 ± 343 m respectively (Table 4). I-DL mean length was longest in the West region ($\overline{X}$ = 829 ± 610 m) and shortest in the Central region ($\overline{X}$ = 549 ± 264 m), while DDA mean length was longest in the Far-west region ($\overline{X}$ = 662 ± 359 m) and shortest in the East region at 413 ± 203 m (Table 4).

Median values (as opposed to means) are reported in order to analyse spatially the landform length, since this variable is not normally distributed and exhibits large standard deviations. Across Nepal, the median landform length of I-DLs (615 m) is greater than that of DDAs (442 m); this pattern is reflected within all sub-regions (Fig. 11a). Additionally, the median length of both I-DLs and DDAs generally increases from east to west (Fig. 11a). Indeed, landform length differed statistically significantly between regions (ANOVA: F-value = 13.42, *df* within groups = 4, between groups = 1132, $p \leq 0.001$).

Tukey post hoc testing of I-DL length (ANOVA: F-value = 5.61, *df* within groups = 4, between groups = 767, $p \leq 0.001$) showed that landforms in the western regions exhibit statistically greater lengths than those in the East region; the West region ($p \leq 0.001$) and Far-west region ($p = 0.010$). Similarly, DDAs (ANOVA: F-value = 6.33, *df* within groups = 4, between groups = 360, $p \leq 0.001$) towards western Nepal are also significantly longer than those situated in eastern Nepal; the Central-west- ($p = 0.043$), West- ($p = 0.001$) and Far-west-regions ($p = 0.030$) DDAs are statistically longer than in the Central region, while those situated in the West region ($p = 0.001$) and Far-west region ($p = 0.037$) are statistically longer than those of the East region. Indeed, the longest observed landform, measuring 4686 m ([5]NEP207_1_11-18-2012), is situated within the Far-west region.

In total, the DDA/I-DL subsample covers 249.83 km^2 of the

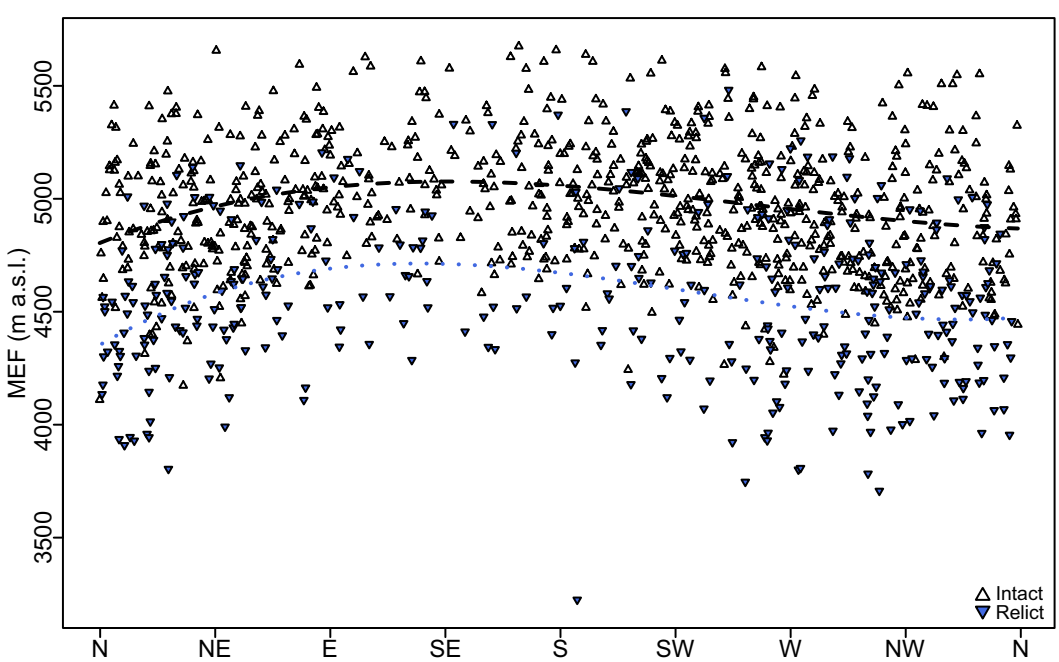

Fig. 7. Scatterplot of mean aspect (°) against MEF showing the distribution of intact and relict landforms Nepal-wide. The two dashed lines are 3rd order polynomial fit (upper line: intact landforms; lower line: relict landforms).

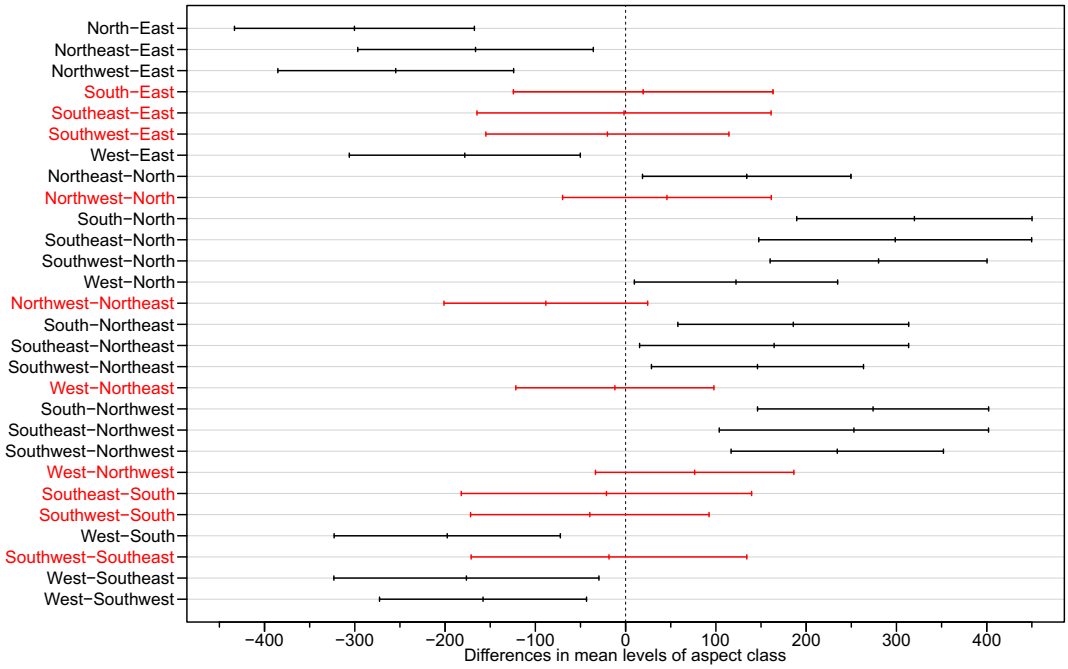

Fig. 8. Tukey post hoc pairwise comparisons of landform MEF as a function of slope aspect class. The plotted lines represent the lower and upper level of the 95% confidence interval around the mean difference (black: statistically significant; red: non-statistically significant). (For interpretation of the references to colour in this figure legend, the reader is referred to the web version of this article.)

Nepalese Himalaya. Furthermore, upscaled estimates total 1371 km^2 throughout Nepal, with regional total upscaled estimates ranging between 43.86 and 731.82 km^2 in the Central- and West-region respectively. Individually, digitised landform area varies between 3.55 and 0.005 km^2, with 719 (~63%) landforms ≥0.1 km^2 in area. Both the largest I-DL and DDA are situated within the West region (3.54 km^2 and 1.50 km^2, respectively). Nepal-wide mean landform area was reported at 0.22 ± 0.30 km^2 and median at 0.13 km^2. There are no DDAs/I-DLs > 1 km^2 in the Central region.

Similar to landform length, regional mean DDA/I-DL area values exhibit large standard deviations and are not normally distributed, thus median values are reported. Overall, median landform area ranges between 0.10 and 0.16 km^2 and generally increases for both DDAs and I-DLs from east to west (Fig. 11b). Furthermore, ANOVA showed statistically significant differences between regions and landform area (F-value = 12.21, *df* within groups = 4, between groups = 1132, $p \leq 0.001$). Tukey post hoc testing of I-DL area (ANOVA: F-value = 6.13, *df* within groups = 4, between groups = 767, $p \leq 0.001$) showed that values in the Central-west- ($p = 0.034$), West- ($p \leq 0.001$) and Far-west-region ($p = 0.013$) were statistically larger than the East region. DDAs (ANOVA: F-value = 3.90, *df* within groups = 4, between groups = 360, $p = 0.004$) in the East region were also found to be statistically smaller than in other regions; the West region ($p = 0.032$) and Far-west region ($p = 0.043$). Conversely, previous work reported the opposite, with landform area in the Nepalese Himalaya decreasing from east to west (Regmi, 2008); however, this study focused on five relatively small-scale study areas across Nepal totalling 1654 km^2.

4.2. Water equivalent volumes

Subsample I-DL thickness estimates ranged between ~19 and ~64 m (mean = ~35 m; Section 3.2.1). Resulting subsample I-DL ice content was estimated to be between 3.35 and 5.03 billion m^3; upscaled I-DL ice content was estimated to be 22.99 ± 0.60 billion m^3 (Table 7).

The results in Table 7 show that the subsample of I-DLs is estimated to contain a total water equivalent volume of 3.81 ± 0.84 km^3 throughout Nepal. The reported upscaled estimates suggest total water volume equivalents of 20.90 ± 4.18 km^3 could reasonably be stored within I-DLs throughout Nepal (see Fig. A.1). Henceforth, I-DL volumetric results will reflect the format *subsample result (upscaled result)*. Regionally, I-DLs within the Central region have been estimated to contain the smallest water volume equivalents, storing between 0.04 and 0.06 km^3 (0.23–0.35 km^3) of water. The East- and Far-west-regions store 0.25 ± 0.05 km^3 (1.31 ± 0.27 km^3) and 0.58 ± 0.12 km^3 (2.99 ± 1.60 km^3) of water respectively, while I-DLs situated within the Central-west region contain frozen hydrological stores between 0.85 and 1.27 km^3 (4.19–6.29 km^3). In the West region, I-DLs contain the largest regional estimated water volume equivalent, 1.57 to2.36 km^3 (8.85–13.27 km^3), more than double the stores within the Central-west region.

GlabTop2 provides estimated ice glacier thicknesses ranging between ~4 and ~454 m (mean = ~49 m; Section 3.2.2) within Nepal, with total ice volume estimated to be ~219.59 billion m^3. On average, I-DLs within the Nepal Himalaya contain 3.81 km^3 (20.90 km^3) of water, whereas ice glaciers store 197.63 km^3 (Tables 7 and 8). This translates to a ratio of I-DL to ice glacier water volume equivalence of 1:52, indicating that ice glaciers store a volume of water ~52 times larger than I-DLs. This ratio reduces to 1:9, where upscaled I-DL water volume equivalents are considered. Regionally, the I-DL to ice glacier water volume equivalent ratio is lowest within the West region, 1:17 (1:3), where I-DLs contain 1.97 km^3 (11.06 km^3) of water compared to 33.67 km^3 stored within ice glaciers. Furthermore, regions west of 84°56′E have lower ratios (Central-west, 1:73 [1:13]; Far-west, 1:26 [1:5]) than those in the East- and Central-regions of Nepal. In the East region, I-DLs contain 0.25 km^3 (1.31 km^3) of water, yet 53.17 km^3 resides within ice glaciers, resulting in an I-DL to ice glacier water volume equivalence ratio of 1:214 (1:40). The highest I-DL to ice glacier water volume equivalence ratio, 1:517 (1:89), aligns with the region containing the fewest number of I-DLs and smallest water volume equivalent – the Central region (0.05 km^3 [0.29 km^3]); ice glacier water volume equivalent in this region is estimated to be 25.86 km^3.

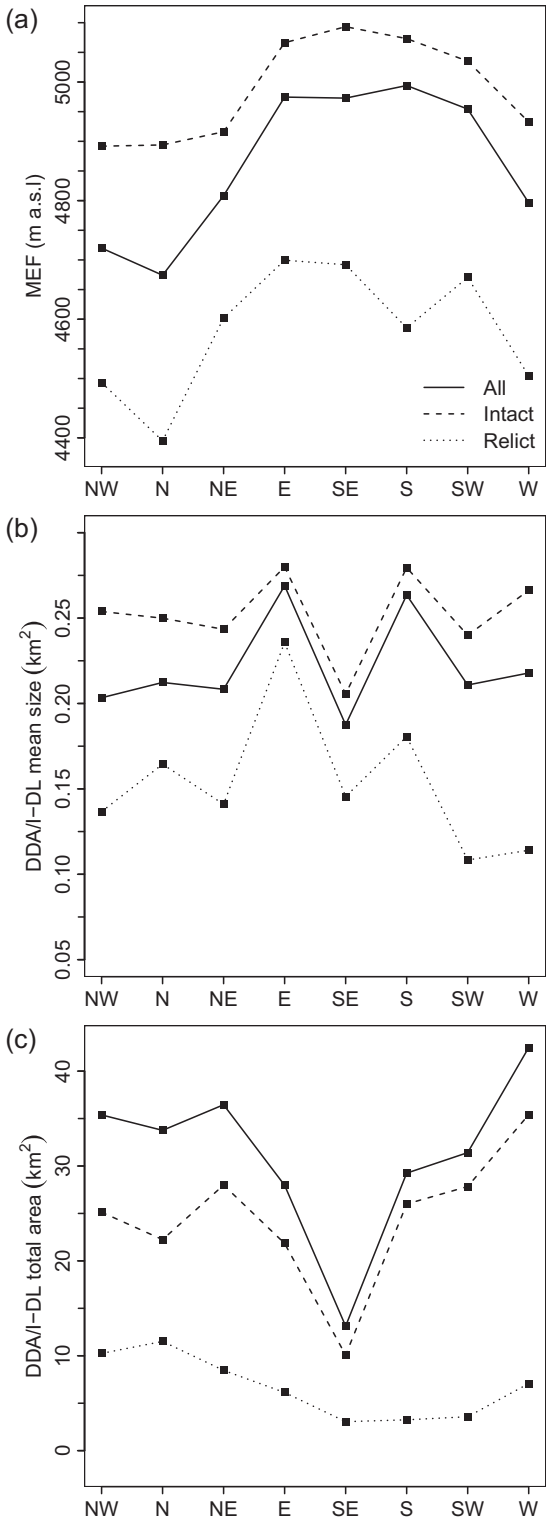

Fig. 9. Analysis of: (a) MEF; (b) DDA/I-DL mean size; and (c) DDA/I-DL total area, as a function of slope aspect.

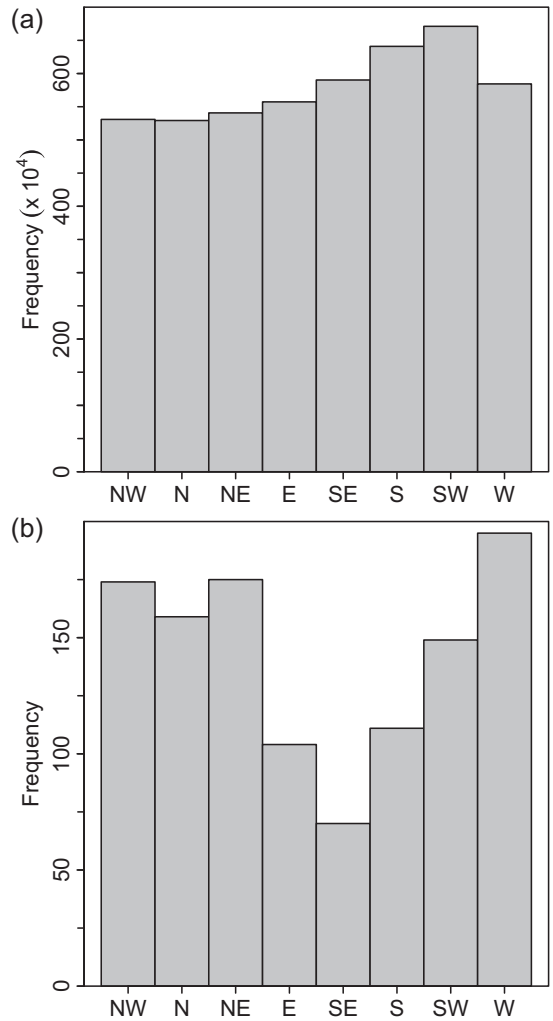

Fig. 10. Analysis of hillslope aspect for landforms in the inventory: (a) frequency of hillslope aspects for all mountain slopes (≥ 3225 m a.s.l.) for each pixel in the Nepalese Himalaya; and (b) frequency of aspect classes for observed landforms in the Nepalese Himalaya.

4.3. Inventory validation

Certainty Index scores, listed in order of occurrence, for the subsample are: *high certainty* (~82%), *virtual certainty* (~11%) and *medium certainty* (~6%). I-DLs dominate the 'virtual certainty' category (96%), while DDAs have a proportionally larger presence in the 'medium certainty' category (63%). This is to be expected. As the geomorphic indicators used to identify DDAs/I-DLs are a surficial expression of the presence of abundant ice (Table 1), relict features (DDAs) or those transitioning towards relict activity status exhibit less well-defined morphological characteristics, and thus increased uncertainty with regards to: (i) clear external boundaries (i.e. outline); (ii) distinct longitudinal flow structure; (iii) distinct transverse flow structure; and (iv) steepness of the frontal slope. To better understand inventory uncertainty, there is a need for further inventory validation beyond those measures (i.e. Certainty Index) already in place.

4.3.1. Comparison with the Permafrost Zonation Index

Rock glaciers, as the most conspicuous morphological manifestation of permafrost in high mountain systems (Barsch, 1996), have previously been utilised for the estimation of permafrost distribution (Janke, 2005; Sattler et al., 2016; Deluigi et al., 2017; Esper Angillieri, 2017). The Global Permafrost Zonation Index (PZI), based on a simple global model with a spatial resolution of ~1 km, is an index that helps to consistently constrain and visualise areas of likely permafrost occurrence (Gruber, 2012). In the HKH region, Schmid et al. (2015) reported good agreement between the PZI and mapped rock glaciers; therefore, here we

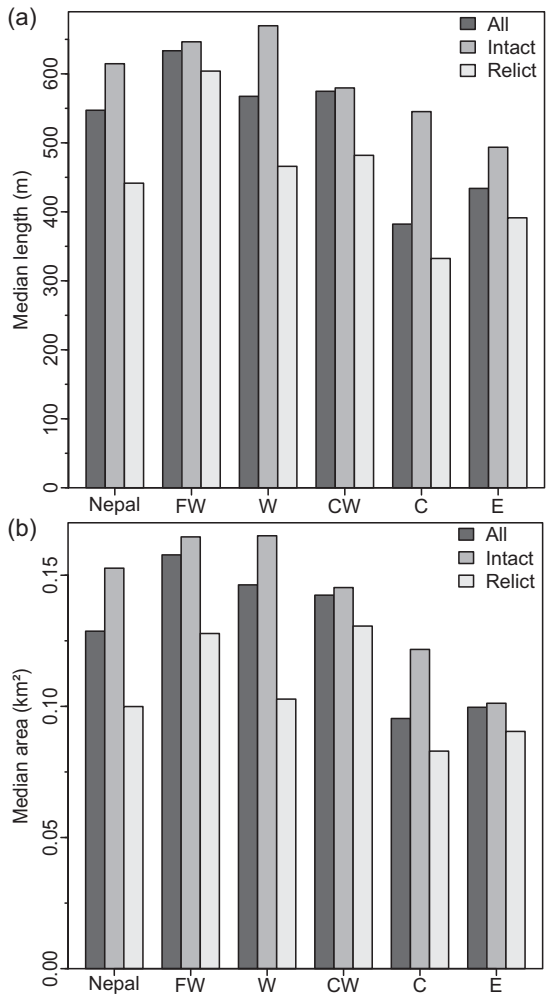

Fig. 11. Nepal-wide- and regional-analysis of DDA/I-DL: (a) median landform length; and (b) median landform area.

Table 7
Ice volume (km^3) and corresponding water volume equivalents (km^3) for both the subsample and upscaled I-DLs, regionally and Nepal-wide (total). These calculations encompass a range of ice content by volume estimates with a lower (40%), average (50%) and upper (60%) bound. Values are reported to two decimal places.

Region	Ice content by volume		Subsample I-DLs		Upscaled I-DLs	
			Ice volume (km^3)	WVEQ (km^3)	Ice volume (km^3)	WVEQ (km^3)
East	Lower	40%	0.22	0.20	1.16	1.05
(86°34′–88°12′E)	Average	50%	0.27	0.25	1.45	1.31
	Upper	60%	0.33	0.30	1.73	1.58
Central	Lower	40%	0.04	0.04	0.26	0.23
(84°56′–86°34′E)	Average	50%	0.05	0.05	0.32	0.29
	Upper	60%	0.07	0.06	0.38	0.35
Central-west	Lower	40%	0.85	0.77	4.61	4.19
(83°18′–84°56′E)	Average	50%	1.06	0.96	5.76	5.24
	Upper	60%	1.27	1.16	6.91	6.29
West	Lower	40%	1.73	1.57	9.73	8.85
(81°40′–83°18′E)	Average	50%	2.16	1.97	12.17	11.06
	Upper	60%	2.60	2.36	14.60	13.27
Far-west	Lower	40%	0.51	0.46	2.63	2.39
(80°02′–81°40′E)	Average	50%	0.64	0.58	3.29	2.99
	Upper	60%	0.76	0.69	3.95	3.59
Total	Lower	40%	3.35	3.05	18.39	16.72
	Average	50%	4.19	3.81	22.99	20.90
	Upper	60%	5.03	4.57	27.59	25.08

WVEQ = water volume equivalent.

compare the spatial distribution of subsample within Nepal to the PZI.

Overall, only ~4% of the DDA/I-DL subsample reaches areas outside of the PZI boundary; thirty-one relict landforms and 13 intact landforms (Fig. 12a). PZI values ≥0.1 form the *permafrost region* (PR), with PZI < 0.1 attributed to the *PZI fringe of uncertainty* – "the zone of uncertainty over which PZI could extend under conservative estimates" (cf. Table 1 in Gruber, 2012). Here, ninety-nine landforms, predominantly DDAs (82%), are situated within the PZI fringe of uncertainty. Thus, 87% of the DDA/I-DL subsample was situated within the PR; 96% and 69% of I-DLs and DDAs respectively. Additionally, with increasing 'habitat suitability' for DDA/I-DL development and sustainability, i.e. towards PZI = 1, we report largely concurrent increases in I-DL frequency and vice versa for DDAs (Fig. 12a). Furthermore, Fig. 12b reflects the spatial distribution of total landform area as a function of PZI values and suggests a strong relationship between DDA/I-DL habitat suitability and total landform area. Regarding Certainty Index scores, those landforms categorised as high certainty and virtual certainty cluster around PZI values ≥0.6 (~56% and ~71%, respectively). DDAs/I-DLs categorised as medium certainty cluster around PZI values ≤0.3 (59%), which may reflect the less well-defined morphological characteristics of landforms – relict features or those transitioning towards relict activity status – containing lower ice volumes. Based upon this summary evaluation, both the DDA/I-DL identification and mapping, and classification of activity status are in good agreement with the PZI. Additionally, several rock glaciers in the Khumbu region were also validated in the field.

5. Discussion

5.1. Landform distribution and morphology

This Nepalese rock glacier inventory identified > 6000 landforms, from which a randomly selected subsample (n = 1137) was digitised, 772 intact- and 365 relict-landforms. The inter-regional MEF of observed landforms was rather inhomogeneous (Fig. 4), however, regional minimum MEFs, both for DDAs and I-DLs, reflect the trend of reduced MEF from east to west reported in earlier work (Regmi, 2008). Digitised DDAs and I-DLs were situated within an elevation range of 3225–5675 m a.s.l., broadly consistent with that reported for the HKH (3500–5500 m a.s.l.) (Schmid et al., 2015). Onaca et al. (2017) report that rock glaciers in the highest mountain ranges are comparatively larger than those in lower mountain ranges, as the duration of their activity lasted longer in the former. In the Nepalese Himalaya, many landform lengths are similar to the largest examples of rock glaciers found elsewhere, including the Karakoram Himalaya where many exceed 2 km, and some as much as 4 km (Hewitt, 2014: p. 276). The Chon-Aksu (Kalgan Tash, Tien Shan) and Karakoram rock glaciers, for example, are reported to be 3.2 and 3.7 km in length respectively (Bolch and Gorbunov, 2014). Additionally, rock glacier area ($\overline{X}$ = 0.22 km^2) exceeds that of rock glaciers in other mountain ranges (cf. Jones et al., in review). Direct conversion of specific landform area (ha km^{-2}) to specific landform density (%) enables comparison with previous studies. At 3.40%, specific landform density within Nepal is higher than other studies in Central Asia; for example, ~1.50% in the Northern Tien Shan (Kazakhstan/Kyrgyzstan) (Bolch and Gorbunov, 2014) and 2.65% in the Zailyiskiy and Kungey Alatau (Kazakhstan/Kyrgyzstan) (Bolch and Marchenko, 2006). However, even higher densities have been reported in the Andes of Santiago (6.70%) and Andes of Mendoza, Chile (5.00%, Brenning, 2005a), and Turtmanntal, Swiss Alps (4.00%, Nyenhuis et al., 2005).

Rock glacier 'habitats' are typically situated in regions with high elevation, low mean annual air temperature and mainly low precipitation (Barsch, 1977; Haeberli, 1983; Baroni et al., 2004); conditions characteristic of the Nepalese Himalaya. At the regional-scale, precipitation and temperature climatically control rock glacier

Table 8
Regional and Nepal-wide area (km^2) and associated water volume equivalents (km^3) for I-DLs (subsample and upscaled) and ice glaciers. Additionally, the I-DL to ice glacier ratios are directly compared. I-DL water volume equivalents assume the 50% (average) ice content by volume. Values are reported to two decimal places.

Region	Regional area (km^2)	Ice-debris landform		Ice glacier		Ratio: I-DL: Ice glacier WVEQ	
		Subsample WVEQ (km^3)	Upscaled WVEQ (km^3)	Area (km^2)	WVEQ (km^3)	Subsample ratio	Upscaled ratio
East	~26,000	0.25	1.31	1013.82	53.17	1:214	1:40
Central	~40,000	0.05	0.29	589.63	25.86	1:517	1:89
Central-west	~30,000	0.96	5.24	1585.47	69.98	1:73	1:13
West	~26,500	1.97	11.06	850.14	33.67	1:17	1:3
Far-west	~25,000	0.58	2.99	386.89	14.95	1:26	1:5
Total	~147,500	3.81	20.90	4425.96	197.63	1:52	1:9

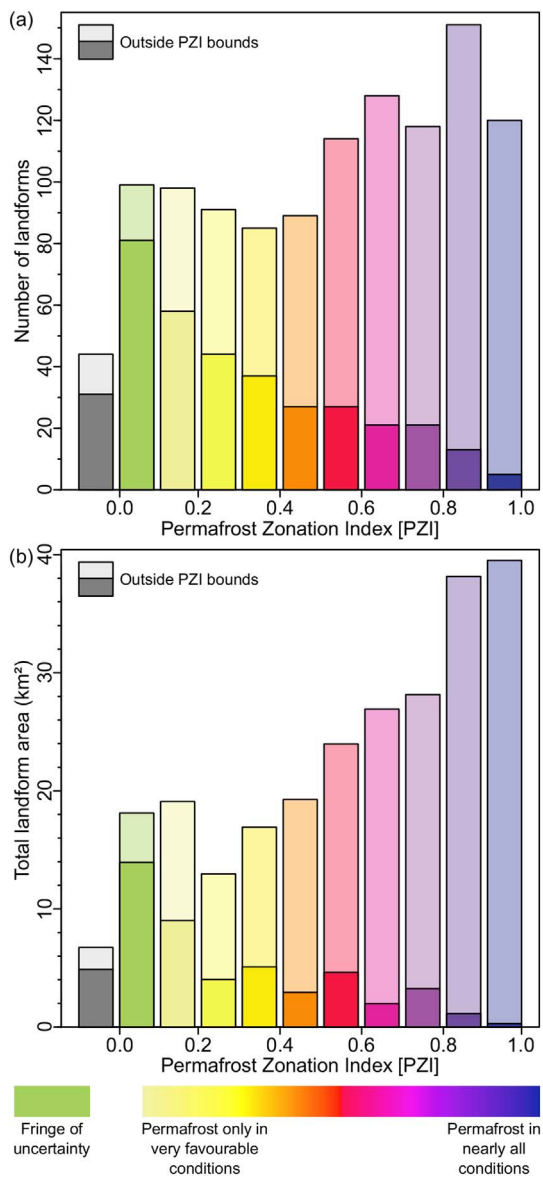

Fig. 12. Analysis of the DDA/I-DL subsample in relation to the Permafrost Zonation Index (PZI) for: (a) number of landforms; and (b) the total landform area. Pale colours represent intact (I-DL) landforms and intense colours indicate relict (DDA) landforms; bars are stacked. Regarding the PZI, see Gruber (2012) for further information.

distribution; the former is dependent on elevation and aspect (Rangecroft et al., 2014).

The 0 °C isotherm of mean annual air temperature (MAAT) and the equilibrium line altitude (ELA) form the lower- and upper-bounds respectively, of I-DL development (Humlum, 1988; Brenning, 2005a; Rangecroft et al., 2014; Rangecroft et al., 2016). The mean MEF difference between intact and relict landforms, therefore, reflects an upward shift (~436 m) of the 0 °C isotherm of MAAT over time. Across the Nepalese Himalaya, precipitation contributions decrease from east to west and from south to north (Kansakar et al., 2004), for instance, regions north of high mountains are particularly arid (< 500 mm year^{-1}) compared to regions located on the windward side (Böhner et al., 2015 as cited in Karki et al., 2017). Furthermore, the lowest precipitation amounts are reported in Mustang, Manang and Dolpa (< 150 mm year^{-1}), situated in the leeward side of the Annapurna Range (Karki et al., 2017). In response to increasing continentality, the ELA increases, expanding the rock glacier niche (e.g., Rangecroft et al., 2014). Barsch and Jakob (1998) note that rock glaciers occur less frequently in subtropical mountain ranges associated with monsoon-dominated climates. In these zones, low snow lines and low ELAs result in extensive glaciation and thus restrict the niche appropriate for rock glacier development. Indeed, the largest and smallest ranges of DDA/I-DL MEFs occur in the West- and Central-regions respectively (Fig. 4), and DDA/I-DL spatial density reflects this trend, with higher values towards the west of Nepal (Table 5). An inverse relationship is apparent between DDA/I-DL occurrence and precipitation, where high DDA/I-DL spatial densities are coupled with drier conditions. Similar assertions have been made for the European Alps (Boeckli et al., 2012). It should be noted, however, that under future warming the 0 °C isotherm may move closer to, or above, mountain summits (Azócar and Brenning, 2010). The resulting smaller rock glacier niche, therefore, potentially leads to decreased frequency in intact landforms and vice versa regarding relict landforms (Krainer and Ribis, 2012).

In the Nepalese Himalaya, analysis of observed landforms as a function of slope aspect confirms that DDAs/I-DLs situated within the north- to west-aspect classes, occur at lower MEFs than those found within the south- to east-aspect classes (Fig. 8), corroborating findings from prior northern hemispheric studies which have found similar relationships (e.g., Seppi et al., 2012; Scotti et al., 2013). Furthermore, this finding is in agreement with previous work in the Kangchenjunga Himal, eastern Nepal, where the lowermost occurrences of rock glaciers were reported to vary from 4800 m a.s.l. on northern slope aspects to 5300 m a.s.l. on south- to east-facing slopes (Ishikawa et al., 2001). Therefore, northerly- and westerly-aspects with their reduced insolation, enable rock glacier formation and preservation at lower MEFs than other aspects (Fig. 7). Furthermore, northerly aspects favour DDA/I-DL occurrence (Table 6), although there was no significant difference in

landform frequency between aspects. Indeed, our results differ from previous inventories in the northern hemisphere (e.g., Barsch, 1996; Guglielmin and Smiraglia, 1997; Baroni et al., 2004) in which observed landforms cluster within the northern quadrant, with < 10% situated in the remaining aspect classes; here, south-facing slopes account for 29% (SW, 13%; S, 10%; SE, 6%) of observed landforms. Although elevation [temperature] is important in determining landform area, no correlation was observed between MEF and DDA/I-DL length ($r = -0.04$) or area ($r = -0.09$). Climatic controls, therefore, only partially explain DDA/I-DL characteristics and distribution.

In addition to climatic conditions, key controls on rock glacier characteristics and distribution include: (i) glacial history (past- and modern-glaciations); and (ii) talus supply (Brenning, 2005a; Johnson et al., 2007). Topographic controls influence rock glacier form and distribution as local terrain, topoclimates and avalanche dynamics may override large-scale climatic- or altitudinal-drivers (Humlum, 1998; Janke, 2007). In the high and deeply incised Himalayas (Scherler et al., 2011), an abundance of steep rock walls associated with glacier-cirques (melted out) and over-deepened valley sides, provides suitable catchment areas for rock glacier development and, combined with intense monsoonal precipitation and tectonic activity, drives sediment transport processes (Barsch and Jakob, 1998). For example, within Central Asia, suggested explanations for rock glacier presence and absence in adjacent valleys of the northern Tien Shan, relate to large earthquake-driven rock avalanches or other mass movements (Gorbunov 1983 in Bolch and Gorbunov, 2014). It is important that lithology, a critical control for talus supply to ice- and rock-glacier surfaces (Haeberli et al., 2006), is evaluated with respect to the above. Unfortunately, high-quality lithological data for the Nepalese Himalaya were not available for use in this study.

5.2. Ice-debris landform water content

Results from the Nepalese Himalaya indicate that I-DLs may act as hydrologically valuable long-term water stores. Studies that consider rock glacier water volume equivalents are limited in number, particularly in Central Asia (Jones et al., in review). Therefore, our estimates are compared to study regions further afield. I-DLs forming the subsample in the Nepalese Himalaya are estimated to store the water volume equivalent of 3.05 to 5.03 km^3, and between 16.72 and 25.08 km^3 when considering upscaled estimates; significantly greater than estimates for other regions, for instance, the Chilean Andes (Azócar and Brenning, 2010), Bolivian Andes (Rangecroft et al., 2015), and the Argentinean Andes (Perucca and Esper Angillieri, 2011). In Chile (27°–33°S), Azócar and Brenning (2010) found 147.5 km^2 of rock glaciers, estimated to store the water equivalent of 2.37 km^3 - exclusive of our estimates, the largest water volume equivalent estimation. Overall, the upscaled national ratio of I-DL to ice glacier water volume equivalent is 1:9 (Table 8), suggesting that as water stores I-DLs in the Nepalese Himalaya are of relatively greater importance than those of the Bolivian Andes, 1:33 (Rangecroft et al., 2015) and the European (Swiss) Alps, ~1:83 (Brenning, 2005a).

However, evaluating the relative hydrological significance of I-DL water volume equivalents with respect to other water stores (e.g., ice glaciers) at the regional-scale vs. the national-scale, provides important information for effective water resource management, particularly in terms of climate change adaptation strategies. Table 8, for instance, shows large inter-regional variability of I-DL water volume equivalents. In the Nepalese Himalaya, both the estimated volumetric ice content and spatial landform density (4.69%) were greatest within the West region, and therefore I-DLs situated in this region have the most potential as water sources. Conversely, volumetric ice content of I-DLs found in the Central region was the lowest in the Nepalese Himalaya. Rangecroft et al. (2015) suggest that through investigating these inter-regional differences in the context of both natural- and anthropogenic-external factors (e.g., population levels and alternate water sources), the hydrological significance of I-DL frozen water storage can be better understood.

5.2.1. Ice-debris landform hydrological significance

Across the Nepalese Himalaya, upscaled estimates of I-DL frozen water stores range between 0.29 and 11.06 km^3 (Tables 7 and 8), with greater volumes found towards the west. I-DLs of the East- and Central-regions stored the lowest amounts of water (1.4% and 6.3% of total estimated I-DL water volume equivalent, respectively), yet with a combined population of ~15.5 million people (~58% of the Nepalese population), these regions are the most densely populated in Nepal (Central Bureau of Statistics, 2014).[1] Within these regions, I-DL to ice glacier water volume equivalent ratios in Table 8 show clearly that I-DLs contribute significantly less to regional water supply than ice glaciers. Central region estimated I-DL water storage is comparable to rock glaciers of the Chilean Andes (27°–29°S), which contain 0.35 km^3 (Azócar and Brenning, 2010), although the relative abundance of other water sources in the Central region, Nepal, suggests I-DLs have lower relative importance than their counterparts in the Chilean Andes (ratio = 1:2.7 [Azócar and Brenning, 2010]). However, we hypothesize that I-DLs will become relatively more important compared to ice glaciers, with continued ice- and debris-covered-glacier mass loss in response to climate change in this region (e.g., Bolch et al., 2012; Kaab et al., 2012; Nuimura et al., 2012; Gardelle et al., 2013; King et al., 2017).

I-DLs are thermally decoupled from external micro- and meso-climates due to the insulative effect of the active layer (Humlum, 1997; Bonnaventure and Lamoureux, 2013; Gruber et al., 2016). Consequently, the response of I-DLs to climate change occurs at decadal time scales, comparatively longer than ice glaciers (Haeberli et al., 2006). Therefore, I-DLs are more climatically resilient than ice glaciers (Millar and Westfall, 2008). Indeed, while I-DL MEFs are often strongly associated with the 0 °C isotherm of MAAT (e.g., Sorg et al., 2015; Rangecroft et al., 2016), examples of I-DLs with positive MAATs have been reported (e.g., Baroni et al., 2004).

Climate-driven deglaciation resulting in the transition from glacial- to paraglacial-dominated process regimes in high mountain systems, for instance, the High Himalaya (Harrison, 2009), may subsequently increase ice glacier surface insulation through enhanced debris-supply (e.g., enhanced rock slope failure), preserving frozen water stores as ice glaciers transition to rock glacier forms (Knight and Harrison, 2014). While few studies have reported the ice- to rock-glacier transition, Monnier and Kinnard (2015) report an example in the Juncal Massif, Chilean central Andes, where the lower-section of the Presenteseracae debris-covered glacier has developed distinctive rock glacier morphology during the previous 60 years. Hillslope-erosion rates and hillslope angle usually increase concomitantly (Ouimet et al., 2009), with increased debris flux to glacier surfaces and therefore formation of debris-covered glaciers linked to steep (> 25°) accumulation areas; topographic characteristics typical within the high and deeply incised Himalayas (Scherler et al., 2011). Indeed, Himalayan debris-covered glaciers commonly have thick debris cover (> 1 m) (Shroder et al., 2000; Nicholson and Benn, 2013). Steady-state talus-nourishment rates to: (i) feature rooting zones encourage rock glacier growth (Bolch and Gorbunov, 2014) and restricts rock glacier starvation (Kellerer-Pirklbauer and Rieckh, 2016); and (ii) glacier surfaces encourages ice- to rock-glacier transition.

I-DLs situated in the Central-west- and West-regions contained the highest amounts of water (25.1% and 52.9% of total estimated I-DL water volume equivalent, respectively) according to our modelling results. In the West region, I-DLs have the highest relative importance as water stores compared to ice glaciers of all regions within the Nepalese

[1] The five geographic sectors used within this study approximately align with the *development regions* used by the Central Bureau of Statistics (2014).

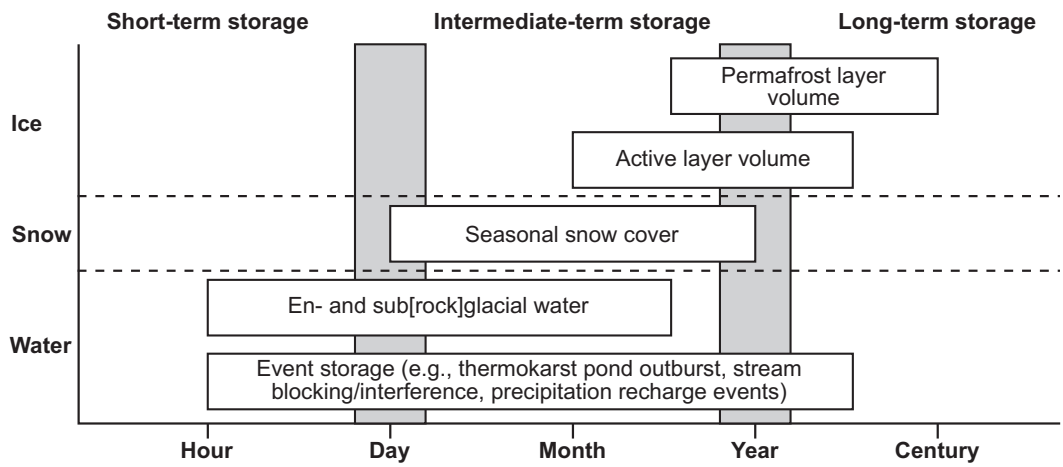

Fig. 13. Schematic diagram showing the different forms of rock glacier storage and their associated time-scales.
Figure adapted from Jansson et al. (2003).

Himalaya, with an I-DL to ice glacier water volume equivalence ratio of 1:3 (Table 8). This ratio is larger than that of the Sajama region, Bolivia (17°–18°S) (Rangecroft et al., 2015) and the Andes of Santiago, Chile (Brenning, 2005a), both with a ratio of 1:7, but of lower importance than in the Semi-arid Chilean Andes (29°–32°S) where rock glaciers are dominant with a ratio of 3:1 (Azócar and Brenning, 2010). Monsoonal precipitation (June–September) dominates annual precipitation (Shrestha et al., 2000; Karki et al., 2016), with contributions decreasing from east to west and from south to north (Kansakar et al., 2004). Consequently, as a result of substantial projected long-term glacial mass losses in response to climate warming (Bolch et al., 2012; Jiménez Cisneros et al., 2014; Huss and Hock, 2015; Shrestha et al., 2015), very low precipitation amounts, and limited investment in water resources infrastructure in mountainous regions (Bartlett et al., 2010, p. 18), we hypothesize that the hydrological value of I-DL water stores towards the west of Nepal, including the Central-west region (1:13), may be of greater importance than the I-DL to ice glacier water volume equivalent ratio initially suggests.

5.2.2. *Further considerations and future research*

Whereas much has been written on the role of ice glaciers in maintaining water supplies (Bradley et al., 2006; Vuille et al., 2008), that of rock glaciers has received comparatively little attention (Duguay et al., 2015). Rock glacier hydrology, however, is highly complex given: "various possible inputs and outputs; phase changes and movement of water associated with the active layer; irregular distribution of frozen matrix that allows convoluted pathways for water flow; and deep crevices into which water disappears, among other complicating factors" (Burger et al., 1999). As a "porous medium that functions as an aquifer having recharge, discharge, through-flow characteristics, and storage" (Burger et al., 1999), 'storage' in rock glaciers occurs at *long-term*, *intermediate term*, and *short-term* timescales (Fig. 13). Within the Nepalese Himalaya, we have shown that I-DLs form long-term stores of frozen water of significant hydrological value; however, the total I-DL water volume equivalents calculated here may not be fully representative of readily available water for human consumption (Duguay et al., 2015; Rangecroft et al., 2015). Importantly, rock glacier hydrological significance relates not solely to the long-term storage of frozen water, but also to: (i) the seasonal storage and release of water; and (ii) the interaction of water flowing through or beneath rock glaciers.

Regarding (i), comparative studies focused on rock glacier- vs. ice glacier-discharge are particularly few in number (Geiger et al., 2014). Within this small body of literature, contrasting perspectives have emerged with regards to the relative significance of rock glacier-derived hydrological contributions, particularly compared to other water sources. Previous studies have reported more consistent discharge from rock glaciers in comparison with ice glaciers (Potter, 1972; Corte, 1987; Gardner and Bajewsky, 1987; Bajewsky and Gardner, 1989). Additionally, rock glacier discharge patterns 'mimic' those of ice glaciers (Krainer and Mostler, 2002; Geiger et al., 2014), although at significantly lower magnitude (Geiger et al., 2014). Others (e.g., Falaschi et al., 2014) report rock glacier hydrological contributions to downstream-runoff are significant; however, these conclusions are based on non-quantitative data (Duguay et al., 2015). Discharge may originate from a single source or multiple sources (e.g., ground ice degradation, ground water discharge near the toe, precipitation events, through-flow of upstream ice- and/or snowpack-derived meltwater) (Burger et al., 1999). Indeed, a negligible or non-measurable contribution of ground ice degradation to discharge has been reported (Cecil et al., 1998; Croce and Milana, 2002; Krainer and Mostler, 2002; Krainer et al., 2007), corroborated by the predominant absence of springs near to the rock glacier toe (i.e. the base of the front slope) in semi-arid regions (Pourrier et al., 2014). However, it is plausible that rock glacier waters may drain directly underground (Pourrier et al., 2014). Discharge-related studies are predominantly focused upon present opposed to potential future rock glacier-derived hydrological contributions; therefore, the hydrological significance of rock glaciers is defined according to a limited time-scale. At decadal and longer time-scales, under future climate warming, thawing of ground ice within rock glaciers may represent an increasing hydrological contribution to downstream regions (Thies et al., 2013). Therefore, we support previous studies (e.g., Duguay et al., 2015) and suggest further quantitative data is required, while field methodologies enabling separation of rock glacier-derived discharge from adjacent water sources are necessary.

Regarding (ii), rock glaciers can strongly influence catchment hydrology. Following precipitation events, total basin hydrographs indicate increased surface runoff within alpine catchments containing rock glaciers, which suggests rock glaciers form impervious surfaces (i.e. the perennially frozen layer at the base of the active layer acts as an aquiclude) (Brenning, 2005b; Geiger et al., 2014). This may increase the likelihood of flooding (Krainer and Mostler, 2002; Geiger et al., 2014). Additionally, rock glaciers are characterised by high storage

capacity (linked to high hydraulic conductivity) and low transmissive function in comparison to ice- and debris-covered-glaciers (Pourrier et al., 2014), particularly features with lower ground ice content. Therefore, rock glaciers can exhibit: (i) a strong buffering effect on the daily-to-monthly variability of transferring glacial- and snowpack-meltwater interflows to downstream areas; and (ii) a high storage capacity that partially delays glacier- and snowpack-meltwater transfer to downstream areas (Pourrier et al., 2014). Consequently, relict rock glaciers may strongly influence catchment hydrology by means of runoff interruption. For example, within the Niedere Tauern Range, Austria, Winkler et al. (2016b) report that following recharge events (i.e. precipitation events), relict rock glaciers rapidly (within hours) release ~20% of their recharge, however the remaining ~80% is considerably delayed; calculated mean residence time is ~0.6 years (≅7 months). Furthermore, exceptionally high discharge rates reported from springs at the toe of relict rock glaciers (Kellerer-Pirklbauer et al., 2013), emphasise the strong influence of this rock glacier type both on the water storage capabilities and discharge behaviour of these catchments. Therefore, relict rock glaciers potentially form 'temporary aquifers' of significant hydrological value; however, they are regularly neglected in the context of rock glacier hydrological significance. Indeed, as yet no scientific investigation has "quantitatively established the complete hydrological role of the periglacial environment within a given watershed or region" (Duguay et al., 2015). Their number, spatial distribution, and morphometric characteristics are defined within this inventory; however, much further research is required to better understand their hydrological role.

With further regards to (ii), given the potential of rock glaciers as potable water sources (Burger et al., 1999), understanding rock glacier outflow water quality characteristics is of critical importance. With slower recessional rates compared to ice glaciers, rock glaciers may influence the biogeochemistry of outflow over comparatively longer time-scales (Fegel et al., 2016). Despite this, the biogeochemistry of rock glacier outflow has been the focus of few scientific investigations. Generally lower suspended sediment concentrations and higher total dissolved solids (TDS) relative to glacier-derived meltwater, have resulted in rock glacier outflow being described as 'clear' (Gardner and Bajewsky, 1987). However, given the greater debris fraction in rock glaciers compared to glaciers, mineral surface area-ground ice contact is greater, and thus undergoes active chemical weathering (Ilyashuk et al., 2014). Indeed, TDS analysis indicates that interflowing waters are chemically influenced with outflows becoming solute-enriched (Giardino et al., 2015). Examples of rock glacier outflow are reported where abnormally high concentrations of certain elements exceed EU limit values for drinking water (e.g., sulphate, manganese, aluminium, nickel [Ilyashuk et al., 2014]). Furthermore, reported outflow pH levels (7.3–8.4) and interflow pH levels (6.4–6.9) (Ilyashuk et al., 2014), further illustrate the 'solute-concentrating effect' of rock glaciers. Others have reported similar findings (Williams et al., 2006; Thies et al., 2007; Nickus et al., 2013; Thies et al., 2013). Therefore, while rock glaciers may form reliable potable water sources, further research into water quality is necessary.

Lastly, in the adaptation context, as "adaption needs are highly diverse, dynamic, and context-specific" (Regmi and Pandit, 2016), particularly in high mountain systems, therefore basin-scale knowledge is critically important. Additionally, research on the impacts of past environmental conditions of the hydrological function of rock glaciers is largely understudied (Sorg et al., 2015); research required to fully understand the applicability of the inventory presented in this study, to future contexts. Finally, under continued climate change many ice glaciers will potentially transition to rock glaciers, however, further research is required to understand this process.

6. Conclusion

In this study, the first complete inventory of DDAs/I-DLs in the Nepalese Himalaya has identified > 6000 features, covering an estimated 1371 km^2. A ~20% subsample (n = 1137) of landforms were digitised, the majority (68%) of which were classified as intact and the remaining as relict. An inverse relationship between precipitation and DDA/I-DL occurrence, elevation and morphometric characteristics (i.e. length and area), with increasing values from east to west associated with drier conditions. Both DDAs and I-DLs situated within north- to west-aspect classes, reside at statistically significantly lower elevations than those within south- to east-aspects. Additionally, the majority (56%) of DDAs and I-DLs had a northerly aspect (NE, N, NW), suggesting that temperature (i.e. solar insolation) is an important control on DDA/I-DL characteristics and distribution. Climatic controls, however, only partially explain DDA/I-DL characteristics and distribution, and thus other controls such as debris supply, glacial history, competition with ice glaciers and lithology should be considered. Indeed, under future climate warming, the hydrological value I-DL frozen water stores in mountain regions is likely to become increasingly important; therefore, improved understanding the controls upon I-DL development is critical. Prior to this study, knowledge of Nepalese I-DL frozen water stores and their hydrological significance at local, regional, and national scales was limited. This study, for the first time, estimates I-DL water volume equivalents and evaluates their relative hydrological importance in comparison to ice glaciers. Across the Nepalese Himalaya, I-DLs stored ~21 trillion L of frozen water, and their comparative hydrological importance increased westwards (e.g., ratio = 1:3, West region). With continued climatically-driven ice glacier recession, the relative importance of I-DLs in the Nepalese Himalaya will potentially increase.

Author contributions

SH, KA and DBJ designed the study. DBJ developed the methodology, identified and 'pinned' DDAs/I-DLs, and undertook the subsequent GIS/statistical analysis. HLS digitised the randomly selected subsample in Google Earth. JLW prepared Figs. 4–7. DBJ wrote the manuscript and prepared the remaining figures, tables and supplementary information files. SH and KA co-edited the manuscript with DBJ and RAB commented on the final manuscript.

Competing interests statement

The authors declare no competing interests, financial or otherwise.

Acknowledgements

This work was supported by the Natural Environment Research Council (grant number: NE/L002434/1 to DBJ); the Royal Geographical Society (with IBG) with a Dudley Stamp Memorial Award (awarded to DBJ); the European Union Seventh Framework Programme FP7/2007–2013 (grant number: 603864 to SH and RAB [HELIX: High-End cLimate Impacts and eXtremes; www.helixclimate.eu]). The work of RB forms part of the BEIS/Defra Met Office Hadley Centre Climate Programme GA01101. The authors would like to thank Himalayan Research Expeditions (P) Ltd. who provided valuable organizational support with regards to the field campaign. We would also like to acknowledge and thank the anonymous reviewers for their constructive comments and suggestions, which improved the manuscript greatly.

Appendix A

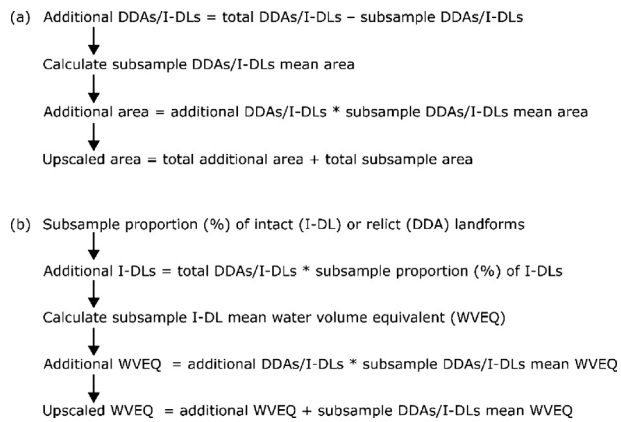

Fig. A.1. Flow diagram detailing the process for: (a) upscaling of DDA/I-DL surface area; and (b) upscaling of DDA/I-DL water volume equivalent. Both are derived from the digitised subsample.

Appendix B. Supplementary data

Supplementary data associated with this article can be found in the online version, at https://doi.org/10.1016/j.gloplacha.2017.11.005. These data include the Google maps of the most important areas described in this article.

References

Alifu, H., Tateishi, R., Johnson, B., 2015. A new band ratio technique for mapping debris-covered glaciers using Landsat imagery and a digital elevation model. Int. J. Remote Sens. 36 (8), 2063–2075.

Allen, S.K., Owens, I., Huggel, C., 2008. A first estimate of mountain permafrost distribution in the Mount Cook region of New Zealand's southern alps. In: 9th International Conference on Permafrost, Fairbanks, Alaska, pp. 37–42.

Azócar, G.F., Brenning, A., 2010. Hydrological and geomorphological significance of rock glaciers in the dry Andes, Chile (27°–33°S). Permafr. Periglac. Process. 21 (1), 42–53.

Azócar, G.F., Brenning, A., Bodin, X., 2016. Permafrost distribution modeling in the semi-arid Chilean Andes. Cryosphere Discuss. 2016, 1–25.

Bahr, D.B., Meier, M.F., Peckham, S.D., 1997. The physical basis of glacier volume-area scaling. J. Geophys. Res. Solid Earth 102 (B9), 20355–20362.

Bajewsky, I., Gardner, J.S., 1989. Discharge and sediment-load characteristics of the Hilda rock-glacier stream, Canadian Rocky Mountains, Alberta. Phys. Geogr. 10 (4), 295–306.

Bajracharya, S.R., Shrestha, B., 2011. The Status of Glaciers in the Hindu Kush-Himalayan Region. ICIMOD, Kathmandu.

Bajracharya, S.R., et al., 2015. The glaciers of the Hindu Kush Himalayas: current status and observed changes from the 1980s to 2010. Int. J. Water Resour. Dev. 31 (2), 161–173.

Baroni, C., Carton, A., Seppi, R., 2004. Distribution and behaviour of rock glaciers in the Adamello–Presanella Massif (Italian Alps). Permafr. Periglac. Process. 15 (3), 243–259.

Barsch, D., 1977. Nature and importance of mass-wasting by rock glaciers in alpine permafrost environments. Earth Surf. Process. 2 (2–3), 231–245.

Barsch, D., 1996. Rockglaciers: Indicators for the Present and Former Geoecology in High Mountain Environments. Springer-Verlag, Berlin, pp. 331.

Barsch, D., Jakob, M., 1998. Mass transport by active rockglaciers in the Khumbu Himalaya. Geomorphology 26 (1–3), 215–222.

Bartlett, R., Bharati, L., Pant, D., Hosterman, H., McCornick, P., 2010. Climate change impacts and adaptation in Nepal. In: International Water Management Institute (IWMI Working Paper 139), Colombo, Sri Lanka, pp. 35.

Berthling, I., 2011. Beyond confusion: rock glaciers as cryo-conditioned landforms. Geomorphology 131 (3–4), 98–106.

Bhambri, R., Bolch, T., 2009. Glacier mapping: a review with special reference to the Indian Himalayas. Prog. Phys. Geogr. 33 (5), 672–704.

Bishop, M.P., et al., 2014. Remote sensing of glaciers in Afghanistan and Pakistan. In: Kargel, S.J., Leonard, J.G., Bishop, P.M., Kääb, A., Raup, H.B. (Eds.), Global Land Ice Measurements from Space. Springer Berlin Heidelberg, Berlin, Heidelberg, pp. 509–548.

Bodin, X., 2013. Present status and development of rock glacier complexes in south-faced valleys (45°N, French Alps). Geogr. Fis. Din. Quat. 36 (2), 27–28.

Boeckli, L., Brenning, A., Gruber, S., Noetzli, J., 2012. A statistical approach to modelling permafrost distribution in the European Alps or similar mountain ranges. Cryosphere 6 (1), 125–140.

Bolch, T., Gorbunov, A.P., 2014. Characteristics and origin of rock glaciers in Northern Tien Shan (Kazakhstan/Kyrgyzstan). Permafr. Periglac. Process. 25 (4), 320–332.

Bolch, T., Kamp, U., 2006. Glacier mapping in high mountains using DEMs, Landsat and ASTER data, Grazer Schriften der Geographie und Raumforschung. In: Proceedings of the 8th International Symposium on High Mountain Remote Sensing Cartography, La Paz, Bolivia, pp. 13–24.

Bolch, T., Marchenko, S.S., 2006. Significance of glaciers, rockglaciers and ice-rich permafrost in the Northern Tien Shan as water towers under climate change conditions. In: Braun, L., Hagg, W., Severskiy, I.V., Young, G.J. (Eds.), Proceedings of the Workshop Assessment of Snow-Glacier and Water Resources in Asia. IHP/HWRP-Berichte, Almaty, Kazakhstan, pp. 132–144.

Bolch, T., et al., 2012. The state and fate of Himalayan glaciers. Science 336 (6079), 310–314.

Bonnaventure, P.P., Lamoureux, S.F., 2013. The active layer: a conceptual review of monitoring, modelling techniques and changes in a warming climate. Prog. Phys. Geogr. 37 (3), 352–376.

Bradley, R.S., Vuille, M., Diaz, H.F., Vergara, W., 2006. Threats to water supplies in the tropical Andes. Science 312 (5781), 1755–1756.

Brazier, V., Kirkbride, M.P., Owens, I.F., 1998. The relationship between climate and rock glacier distribution in the Ben Ohau Range, New Zealand. Geogr. Ann. Ser. A Phys. Geogr. 80 (3–4), 193–207.

Brenning, A., 2005a. Climatic and Geomorphological Controls of Rock Glaciers in the Andes of Central Chile: Combining Statistical Modelling and Field Mapping. Humboldt-Universität zu Berlin, Berlin, Germany.

Brenning, A., 2005b. Geomorphological, hydrological and climatic significance of rock glaciers in the Andes of Central Chile (33–35°S). Permafr. Periglac. Process. 16 (3), 231–240.

Brenning, A., 2009. Benchmarking classifiers to optimally integrate terrain analysis and multispectral remote sensing in automatic rock glacier detection. Remote Sens. Environ. 113 (1), 239–247.

Burger, K.C., Degenhardt Jr, J.J., Giardino, J.R., 1999. Engineering geomorphology of rock glaciers. Geomorphology 31 (1–4), 93–132.

Cecil, L.D., Green, J.R., Vogt, S., Michel, R., Cottrell, G., 1998. Isotopic composition of ice cores and meltwater from Upper Fremont Glacier and Galena Creek rock glacier, Wyoming. Geogr. Ann. Ser. A Phys. Geogr. 80 (3/4), 287–292.

Central Bureau of Statistics, 2014. Population Monograph of Nepal, Volume I - Population Dynamics. National Planning Commission Secretariat, Government of Nepal Kathmandu, Nepal.

Charbonneau, A.A., 2015. Rock Glacier Activity and Distribution in the Southeastern British Columbia Coast Mountains. University of Victoria.

Chen, J., Ohmura, A., 1990. Estimation of Alpine glacier water resources and their change since the 1870s. In: Lang, H., Musy, A. (Eds.), Hydrology in Mountainous Regions. I-Hydrological Measurements. IAHS Press Publications, Oxfordshire, UK, pp. 127–135.

Chueca, J., 1992. A statistical analysis of the spatial distribution of rock glaciers, Spanish Central Pyrenees. Permafr. Periglac. Process. 3 (3), 261–265.

Cogley, J.G., 2011. Present and future states of Himalaya and Karakoram glaciers. Ann. Glaciol. 52 (59), 69–73.

Colucci, R.R., Boccali, C., Žebre, M., Guglielmin, M., 2016. Rock glaciers, protalus ramparts and pronival ramparts in the south-eastern lps. Geomorphology 269, 112–121.

Corte, A.E., 1987. Central Andes rock glaciers: applied aspects. In: Giardino, J.R., Shroder Jr, J.F., Vitek, J.D. (Eds.), Rock Glaciers. Allen and Unwin, London, pp. 289–304.

Cremonese, E., et al., 2011. Brief communication: "An inventory of permafrost evidence for the European Alps". Cryosphere 5 (3), 651–657.

Croce, F.A., Milana, J.P., 2002. Internal structure and behaviour of a rock glacier in the

Arid Andes of Argentina. Permafr. Periglac. Process. 13 (4), 289–299.
Davis, J.C., 2002. Statistics and Data Analysis in Geology. John Wiley & Sons, United States of America.
Deluigi, N., Lambiel, C., Kanevski, M., 2017. Data-driven mapping of the potential mountain permafrost distribution. Sci. Total Environ. 590–591, 370–380.
Duguay, M.A., Edmunds, A., Arenson, L.U., Wainstein, P.A., 2015. Quantifying the significance of the hydrological contribution of a rock glacier - a review. In: GEOQuébec 2015: Challenges From North to South, Québec, Canada.
Ellis, J.M., Calkin, P.E., 1979. Nature and distribution of glaciers, neoglacial moraines, and rock glaciers, east-central Brooks Range, Alaska. Arct. Alp. Res. 11 (4), 403–420.
Esper Angillieri, M.Y., 2009. A preliminary inventory of rock glaciers at 30°S latitude, Cordillera Frontal of San Juan, Argentina. Quat. Int. 195 (1–2), 151–157.
Esper Angillieri, M.Y., 2017. Permafrost distribution map of San Juan Dry Andes (Argentina) based on rock glacier sites. J. S. Am. Earth Sci. 73, 42–49.
Etzelmüller, B., et al., 2007. The regional distribution of mountain permafrost in Iceland. Permafr. Periglac. Process. 18 (2), 185–199.
Falaschi, D., Castro, M., Masiokas, M., Tadono, T., Ahumada, A.L., 2014. Rock glacier inventory of the Valles Calchaquíes Region (~25°S), Salta, Argentina, derived from ALOS data. Permafr. Periglac. Process. 25 (1), 69–75.
Falaschi, D., Tadono, T., Masiokas, M., 2015. Rock glaciers in the Patagonian Andes: an inventory for the Monte San Lorenzo (Cero Cochrane) Massif, 47° S. Geogr. Ann. Ser. A Phys. Geogr. 1–9.
Falaschi, D., Masiokas, M., Tadono, T., Couvreux, F., 2016. ALOS-derived glacier and rock glacier inventory of the Volcán Domuyo region (~36° S), southernmost Central Andes, Argentina. Z. Geomorphol. 60 (3), 195–208.
Fegel, T.S., Baron, J.S., Fountain, A.G., Johnson, G.F., Hall, E.K., 2016. The differing biogeochemical and microbial signatures of glaciers and rock glaciers. J. Geophys. Res. Biogeosci. 121 (3), 919–932.
Frauenfelder, R., Haeberli, W., Hoelzle, M., 2003. Rockglacier occurrence and related terrain parameters in a study area of the Eastern Swiss Alps. In: Proceedings 8th International Conference on Permafrost. Swets and Zeitlinger, Lisse, pp. 253–258.
Frehner, M., Ling, A.H.M., Gärtner-Roer, I., 2015. Furrow-and-ridge morphology on rockglaciers explained by gravity-driven buckle folding: a case study from the Murtèl rockglacier (Switzerland). Permafr. Periglac. Process. 26 (1), 57–66.
Frey, H., et al., 2014. Estimating the volume of glaciers in the Himalayan-Karakoram region using different methods. Cryosphere 8 (6), 2313–2333.
Gardelle, J., Berthier, E., Arnaud, Y., Kääb, A., 2013. Region-wide glacier mass balances over the Pamir-Karakoram-Himalaya during 1999–2011. Cryosphere 7, 1263–1286.
Gardner, J.S., Bajewsky, I., 1987. Hilda rock glacier stream discharge and sediment load characteristics, Sunwapta Pass area, Canadian Rocky Mountains. In: Giardino, J.R., Shroder Jr, J.F., Vitek, J.D. (Eds.), Rock Glaciers. Allen and Unwin, London, pp. 161–174.
Gardner, A.S., et al., 2013. A reconciled estimate of glacier contributions to sea level rise: 2003 to 2009. Science 340 (6134), 852–857.
Geiger, S.T., Daniels, J.M., Miller, S.N., Nicholas, J.W., 2014. Influence of rock glaciers on stream hydrology in the La Sal Mountains, Utah. Arct. Antarct. Alp. Res. 46 (3), 645–658.
Giardino, M., et al., 2015. Chemical and physical characterisation of water in an alpine permafrost area (Col d'Olen LTER site, Italian NW-Alps). Geophys. Res. Abstr. 17, 13744.
Gleick, P.H., Palaniappan, M., 2010. Peak water limits to freshwater withdrawal and use. Proc. Natl. Acad. Sci. 107 (25), 11155–11162.
Gorbunov, A.P., Titkov, S.N., Polyakov, V.G., 1992. Dynamics of rock glaciers of the Northern Tien Shan and the Djungar Ala Tau, Kazakhstan. Permafr. Periglac. Process. 3 (1), 29–39.
Gorbunov, A.P., Seversky, E.V., Titkov, S.N., Marchenko, S.S., Popov, M., 1998. In: NSIDC (Ed.), Rock glaciers, Zailiysiky Range, Kungei Ranges, Tienshan, Kazakhstan. Digital Media, Boulder, CO.
Grinsted, A., 2013. An estimate of global glacier volume. Cryosphere 7 (1), 141–151.
Gruber, S., 2012. Derivation and analysis of a high-resolution estimate of global permafrost zonation. Cryosphere 6 (1), 221–233.
Gruber, S., et al., 2016. Review article: inferring permafrost and permafrost thaw in the mountains of the Hindu Kush Himalaya region. Cryosphere Discuss. 2016, 1–29.
Guglielmin, M., Smiraglia, C., 1997. Rock glacier inventory of the Italian Alps. Italian Glaciological Committee Archives 3, 117.
Guglielmin, M., Smiraglia, C., 1998. The Rock Glacier Inventory of the Italian Alps. In: Permafrost - Seventh International Conference (Proceedings). Collection Nordicana, Yellowknife (Canada).
Haeberli, W., 1983. Permafrost-glacier relationships in the Swiss Alps - today and in the past. In: Permafrost Fourth International Conference, NAP/Washington D.C. pp. 415–420.
Haeberli, W., et al., 1998. Ten years after drilling through the permafrost of the active rock glacier Murtèl, eastern Swiss Alps: answered questions and new perspectives. In: 7th International Conference on Permafrost. Proceedings, Yellowknife, pp. 403–410.
Haeberli, W., et al., 2006. Permafrost creep and rock glacier dynamics. Permafr. Periglac. Process. 17 (3), 189–214.
Harrison, S., 2009. Climate sensitivity: implications for the response of geomorphological systems to future climate change. In: Knight, J., Harrison, S. (Eds.), Periglacial and Paraglacial Processes and Environments. Geological Society of London, London, pp. 257–265.
Harrison, S., Whalley, B., Anderson, E., 2008. Relict rock glaciers and protalus lobes in the British Isles: implications for Late Pleistocene mountain geomorphology and palaeoclimate. J. Quat. Sci. 23 (3), 287–304.
Hausmann, H., Krainer, K., Brückl, E., Ullrich, C., 2012. Internal structure, ice content and dynamics of Ölgrube and Kaiserberg rock glaciers (Ötztal Alps, Austria) determined from geophysical surveys. Aust. J. Earth Sci. 105 (2), 12–31.
Hewitt, K., 2014. Rock glaciers and related phenomena. In: Glaciers of the Karakoram Himalaya: Glacial Environments, Processes, Hazards and Resources. Springer Netherlands, Dordrecht, pp. 267–289.
Humlum, O., 1988. Rock glacier appearance level and rock glacier initiation line altitude: a methodological approach to the study of rock glaciers. Arct. Alp. Res. 20 (2), 160–178.
Humlum, O., 1997. Active layer thermal regime at three rock glaciers in Greenland. Permafr. Periglac. Process. 8 (4), 383–408.
Humlum, O., 1998. The climatic significance of rock glaciers. Permafr. Periglac. Process. 9 (4), 375–395.
Humlum, O., 2000. The geomorphic significance of rock glaciers: estimates of rock glacier debris volumes and headwall recession rates in West Greenland. Geomorphology 35 (1–2), 41–67.
Huss, M., Farinotti, D., 2012. Distributed ice thickness and volume of all glaciers around the globe. J. Geophys. Res. Earth Surf. 117 (F4).
Huss, M., Hock, R., 2015. A new model for global glacier change and sea-level rise. Front. Earth Sci. 3 (54).
Ilyashuk, B.P., Ilyashuk, E.A., Psenner, R., Tessadri, R., Koinig, K.A., 2014. Rock glacier outflows may adversely affect lakes: lessons from the past and present of two neighboring water bodies in a crystalline-rock watershed. Environ. Sci. Technol. 48 (11), 6192–6200.
Imhof, M., 1996. Modelling and verification of the permafrost distribution in the Bernese Alps (Western Switzerland). Permafr. Periglac. Process. 7 (3), 267–280.
Immerzeel, W.W., van Beek, L.P.H., Bierkens, M.F.P., 2010. Climate change will affect the Asian water towers. Science 328 (5984), 1382–1385.
Ishikawa, M., Watanabe, T., Nakamura, N., 2001. Genetic differences of rock glaciers and the discontinuous mountain permafrost zone in Kanchanjunga Himal, Eastern Nepal. Permafr. Periglac. Process. 12 (3), 243–253.
Jakob, M., 1992. Active rock glaciers and the lower limit of discontinuous alpine permafrost, Khumbu Himalaya, Nepal. Permafr. Periglac. Process. 3 (3), 253–256.
Janke, J.R., 2005. Modeling past and future alpine permafrost distribution in the Colorado Front Range. Earth Surf. Process. Landf. 30 (12), 1495–1508.
Janke, J.R., 2007. Colorado Front Range rock glaciers: distribution and topographic characteristics. Arct. Antarct. Alp. Res. 39 (1), 74–83.
Janke, J.R., 2013. Using airborne LiDAR and USGS DEM data for assessing rock glaciers and glaciers. Geomorphology 195, 118–130.
Janke, J.R., Regmi, N.R., Giardino, J.R., Vitek, J.D., 2013. Rock glaciers. In: Shroder, J., Giardino, R., Harbor, J. (Eds.), Treatise on Geomorphology. Academic Press, San Diego, CA, pp. 238–273.
Janke, J.R., Bellisario, A.C., Ferrando, F.A., 2015. Classification of debris-covered glaciers and rock glaciers in the Andes of central Chile. Geomorphology 241, 98–121.
Janke, J.R., Ng, S., Bellisario, A., 2017. An inventory and estimate of water stored in firn fields, glaciers, debris-covered glaciers, and rock glaciers in the Aconcagua River Basin, Chile. Geomorphology 296, 142–152.
Jansson, P., Hock, R., Schneider, T., 2003. The concept of glacier storage: a review. J. Hydrol. 282 (1–4), 116–129.
Jarman, D., Wilson, P., Harrison, S., 2013. Are there any relict rock glaciers in the British mountains? J. Quat. Sci. 28 (2), 131–143.
Jiménez Cisneros, B.E., et al., 2014. Freshwater resources. In: Field, C.B. (Ed.), Climate Change 2014: Impacts, Adaptation, and Vulnerability. Part A: Global and Sectoral Aspects. Contribution of Working Group II to the Fifth Assessment Report of the Intergovernmental Panel on Climate Change. Cambridge University Press, Cambridge, United Kingdom and New York, NY, USA, pp. 229–269.
Johnson, B.G., Thackray, G.D., Van Kirk, R., 2007. The effect of topography, latitude, and lithology on rock glacier distribution in the Lemhi Range, central Idaho, USA. Geomorphology 91 (1–2), 38–50.
Jones, D.B., 2017. Data for: The distribution and hydrological significance of rock glaciers in the Nepalese Himalaya. Mendeley Data.
Kääb, A., Weber, M., 2004. Development of transverse ridges on rock glaciers: field measurements and laboratory experiments. Permafr. Periglac. Process. 15 (4), 379–391.
Kaab, A., Berthier, E., Nuth, C., Gardelle, J., Arnaud, Y., 2012. Contrasting patterns of early twenty-first-century glacier mass change in the Himalayas. Nature 488 (7412), 495–498.
Kansakar, S.R., Hannah, D.M., Gerrard, J., Rees, G., 2004. Spatial pattern in the precipitation regime of Nepal. Int. J. Climatol. 24 (13), 1645–1659.
Karki, R., Talchabhadel, R., Aalto, J., Baidya, S.K., 2016. New climatic classification of Nepal. Theor. Appl. Climatol. 125 (3), 799–808.
Karki, R., Hasson, S., Schickhoff, U., Scholten, T., Böhner, J., 2017. Rising precipitation extremes across Nepal. Climate 5 (1), 4.
Kellerer-Pirklbauer, A., Rieckh, M., 2016. Monitoring nourishment processes in the rooting zone of an active rock glacier in an alpine environment. Z. Geomorphol. Suppl. Iss. 60 (3), 99–121.
Kellerer-Pirklbauer, A., Pauritsch, M., Winkler, G., 2013. Relict rock glaciers in alpine catchments: a regional study in Central Austria. Geophys. Res. Abstr. 15, EGU2013–8467.
King, O., Quincey, D.J., Carrivick, J.L., Rowan, A.V., 2017. Spatial variability in mass loss of glaciers in the Everest region, central Himalayas, between 2000 and 2015. Cryosphere 11 (1), 407–426.
Knight, J., Harrison, S., 2014. Glacial and paraglacial environments. Geogr. Ann. Ser. A Phys. Geogr. 96 (3), 241–244.
Kohler, T., Wehrli, A., Jurek, M., 2014. Mountains and climate change: a global concern. In: Sustainable Mountain Development Series. Centre for Development and Environment (CDE), Swiss Agency for Development and Cooperation (SDC) and Geographica Bernensia, Bern, Switzerland (136 pp).
Krainer, K., Mostler, W., 2002. Hydrology of active rock glaciers: examples from the

Austrian Alps. Arct. Antarct. Alp. Res. 34 (2), 142–149.
Krainer, K., Ribis, M., 2012. A rock glacier inventory of the Tyrolean Alps (Austria). Aust. J. Earth Sci. 105 (2), 32–47.
Krainer, K., Mostler, W., Spötl, C., 2007. Discharge from active rock glaciers, Austrian Alps: a stable isotope approach. Aust. J. Earth Sci. 100, 102–112.
Legg, B.N., 2016. Rock Glacier Morphology and Morphometry in Glacier National Park, Northwest Montana, USA. Texas State University (Masters Thesis Thesis, 77 pp).
Lilleøren, K.S., Etzelüller, B., 2011. A regional inventory of rock glaciers and ice-cored moraines in Norway. Geogr. Ann. Ser. A Phys. Geogr. 93 (3), 175–191.
Linsbauer, A., Paul, F., Hoelzle, M., Frey, H., Haeberli, W., 2009. The Swiss Alps without glaciers – a GIS-based modelling approach for reconstruction of glacier beds. In: Purves, R., Gruber, S., Straumann, R., Hengl, T. (Eds.), Proceedings of Geomorphometry 2009. University of Zurich, Zurich, Switzerland, pp. 243–247.
Liu, L., Millar, C.I., Westfall, R.D., Zebker, H.A., 2013. Surface motion of active rock glaciers in the Sierra Nevada, California, USA: inventory and a case study using InSAR. Cryosphere 7 (4), 1109–1119.
Marzeion, B., Jarosch, A.H., Hofer, M., 2012. Past and future sea-level change from the surface mass balance of glaciers. Cryosphere 6 (6), 1295–1322.
Millar, C.I., Westfall, R.D., 2008. Rock glaciers and related periglacial landforms in the Sierra Nevada, CA, USA; inventory, distribution and climatic relationships. Quat. Int. 188 (1), 90–104.
Monnier, S., Kinnard, C., 2015. Reconsidering the glacier to rock glacier transformation problem: new insights from the central Andes of Chile. Geomorphology 238, 47–55.
Nicholson, L., Benn, D.I., 2013. Properties of natural supraglacial debris in relation to modelling sub-debris ice ablation. Earth Surf. Process. Landf. 38 (5), 490–501.
Nickus, U., et al., 2013. Rock Glacier Äußeres Hochebenkar (Austria) – recent results of a monitoring network. Z. Gletscherk. Glazialgeol. 47, 43–62.
Nuimura, T., Fujita, K., Yamaguchi, S., Sharma, R.R., 2012. Elevation changes of glaciers revealed by multitemporal digital elevation models calibrated by GPS survey in the Khumbu region, Nepal Himalaya, 1992–2008. J. Glaciol. 58 (210), 648–656.
Nyenhuis, M., Hoelzle, M., Dikau, R., 2005. Rock glacier mapping and permafrost distribution modelling in the Turtmanntal, Valais, Switzerland. Zeitschrift Fur Geomorphologie 49 (3), 275–292.
Onaca, A., Ardelean, F., Urdea, P., Magori, B., 2017. Southern Carpathian rock glaciers: inventory, distribution and environmental controlling factors. Geomorphology 293 (Part B), 391–404.
Ouimet, W.B., Whipple, K.X., Granger, D.E., 2009. Beyond threshold hillslopes: channel adjustment to base-level fall in tectonically active mountain ranges. Geology 37 (7), 579–582.
Owen, L.A., England, J., 1998. Observations on rock glaciers in the Himalayas and Karakoram Mountains of northern Pakistan and India. Geomorphology 26 (1–3), 199–213.
Page, A., 2009. A Topographic and Photogrammetric Study of Rock Glaciers in the Southern Yukon Territory. University of Ottawa (168 pp).
Paterson, W.S.B., 1994. The Physics of Glaciers. Butterworth-Heinemann, Oxford.
Paul, F., et al., 2009. Recommendations for the compilation of glacier inventory data from digital sources. Ann. Glaciol. 50 (53), 119–126.
Perucca, L., Esper Angillieri, Y., 2008. A preliminary inventory of periglacial landforms in the Andes of La Rioja and San Juan, Argentina, at about 28°S. Quat. Int. 190 (1), 171–179.
Perucca, L., Esper Angillieri, M., 2011. Glaciers and rock glaciers' distribution at 28° SL, Dry Andes of Argentina, and some considerations about their hydrological significance. Environ. Earth Sci. 64 (8), 2079–2089.
Potter, N., 1972. Ice-cored rock glacier, Galena Creek, northern Absaroka Mountains, Wyoming. Geol. Soc. Am. Bull. 83 (10), 3025–3058.
Potter, N., et al., 1998. Galena Creek rock glacier revisited - new observations on an old controversy. Geogr. Ann. Ser. A Phys. Geogr. 80A (3–4), 251–265.
Pourrier, J., Jourde, H., Kinnard, C., Gascoin, S., Monnier, S., 2014. Glacier meltwater flow paths and storage in a geomorphologically complex glacial foreland: the case of the Tapado glacier, dry Andes of Chile (30°S). J. Hydrol. 519 (Part A), 1068–1083.
Rangecroft, S., et al., 2014. A first rock glacier inventory for the Bolivian Andes. Permafr. Periglac. Process. 25 (4), 333–343.
Rangecroft, S., Harrison, S., Anderson, K., 2015. Rock glaciers as water stores in the Bolivian Andes: an assessment of their hydrological importance. Arct. Antarct. Alp. Res. 47 (1), 89–98.
Rangecroft, S., Suggitt, A.J., Anderson, K., Harrison, S., 2016. Future climate warming and changes to mountain permafrost in the Bolivian Andes. Clim. Chang. 137 (1), 231–243.
Regmi, D., 2008. Rock Glacier distribution and the lower limit of discontinuous mountain permafrost in the Nepal Himalaya. In: Proceedings of the Ninth International Conference on Permafrost, Fairbanks, Alaska, pp. 1475–1480.
Regmi, B.R., Pandit, A., 2016. Classification of adaptation measures in criteria for evaluation: case studies in the Gandaki River Basin. In: HI-AWARE Working Paper 6. HI-AWARE, Kathmandu.
Roer, I., Nyenhuis, M., 2007. Rockglacier activity studies on a regional scale: comparison of geomorphological mapping and photogrammetric monitoring. Earth Surf. Process. Landf. 32 (12), 1747–1758.
Salvador-Franch, F., Pérez-Sánchez, J., Salvà-Catarineu, M., Gómez-Ortiz, A., 2016. Inventory and spatial distribution of rock glaciers in the Eastern Pyrenees: paleoenvironmental implications. Geophys. Res. Abstr. 18 (EGU2016-16284).
Sattler, K., Anderson, B., Mackintosh, A., Norton, K., de Róiste, M., 2016. Estimating permafrost distribution in the maritime Southern Alps, New Zealand, based on climatic conditions at rock glacier sites. Front. Earth Sci. 4.
Scherler, D., Bookhagen, B., Strecker, M.R., 2011. Spatially variable response of Himalayan glaciers to climate change affected by debris cover. Nat. Geosci. 4 (3), 156–159.
Schmid, M.O., et al., 2015. Assessment of permafrost distribution maps in the Hindu Kush Himalayan region using rock glaciers mapped in Google Earth. Cryosphere 9 (6), 2089–2099.
Scotti, R., Brardinoni, F., Alberti, S., Frattini, P., Crosta, G.B., 2013. A regional inventory of rock glaciers and protalus ramparts in the central Italian Alps. Geomorphology 186, 136–149.
Seligman, Z.M., 2009. Rock-Glacier Distribution, Activity, and Movement, Northern Absaroka and Beartooth Ranges, MT, USA. University of Montana, Missoula, MT (63 pp).
Seppi, R., et al., 2012. Inventory, distribution and topographic features of rock glaciers in the southern region of the Eastern Italian Alps (Trentino). Geogr. Fis. Din. Quat. 35 (2), 185–197.
Shrestha, M.L., 2000. Interannual variation of summer monsoon rainfall over Nepal and its relation to Southern Oscillation Index. Meteorog. Atmos. Phys. 75 (1), 21–28.
Shrestha, A.B., Aryal, R., 2011. Climate change in Nepal and its impact on Himalayan glaciers. Reg. Environ. Chang. 11 (1), 65–77.
Shrestha, A.B., Joshi, S.P., 2011. Snow cover and glacier change study in Nepalese Himalaya using remote sensing and geographic information system. J. Hydrol. Meteorol. 6 (1), 11.
Shrestha, A.B., Wake, C.P., Dibb, J.E., Mayewski, P.A., 2000. Precipitation fluctuations in the Nepal Himalaya and its vicinity and relationship with some large scale climatological parameters. Int. J. Climatol. 20 (3), 317–327.
Shrestha, A.B. et al., 2015. The Himalayan Climate and Water Atlas: Impact of climate change on water resources in five of Asia's major river basins. ICIMOD, GRID-Arendal and CICERO.
Shroder, J.F., Bishop, M.P., Copland, L., Sloan, V.F., 2000. Debris-covered glaciers and rock glaciers in the Nanga Parbat Himalaya, Pakistan. Geogr. Ann. Ser. A Phys. Geogr. 82 (1), 17–31.
Shukla, A., Ali, I., 2016. A hierarchical knowledge-based classification for glacier terrain mapping: a case study from Kolahoi Glacier, Kashmir Himalaya. Ann. Glaciol. 57 (71), 1–10.
Shukla, A., Arora, M.K., Gupta, R.P., 2010. Synergistic approach for mapping debris-covered glaciers using optical–thermal remote sensing data with inputs from geomorphometric parameters. Remote Sens. Environ. 114 (7), 1378–1387.
Sollid, J.L., Sørbel, L., 1992. Rock glaciers in Svalbard and Norway. Permafr. Periglac. Process. 3 (3), 215–220.
Sorg, A., Huss, M., Rohrer, M., Stoffel, M., 2014a. The days of plenty might soon be over in glacierized Central Asian catchments. Environ. Res. Lett. 9 (10), 104018.
Sorg, A., et al., 2014b. Coping with changing water resources: the case of the Syr Darya river basin in Central Asia. Environ. Sci. Pol. 43, 68–77.
Sorg, A., Kääb, A., Roesch, A., Bigler, C., Stoffel, M., 2015. Contrasting responses of Central Asian rock glaciers to global warming. Sci. Rep. 5, 8228.
Springman, S.M., et al., 2012. Multidisciplinary investigations on three rock glaciers in the Swiss Alps: legacies and future perspectives. Geogr. Ann. Ser. A Phys. Geogr. 94 (2), 215–243.
Thies, H., et al., 2007. Unexpected response of high alpine lake waters to climate warming. Environ. Sci. Technol. 41 (21), 7424–7429.
Thies, H., Nickus, U., Tolotti, M., Tessadri, R., Krainer, K., 2013. Evidence of rock glacier melt impacts on water chemistry and diatoms in high mountain streams. Cold Reg. Sci. Technol. 96, 77–85.
Triglav-Čekada, M., Barkorič, B., Ferk, M., Zorn, M., 2016. Nationwide aerial laser scanning reveals relict rock glaciers and protalus ramparts in Slovenia. Cryosphere Discuss. 2016, 1–17.
Udmale, P., Ishidaira, H., Thapa, B., Shakya, N., 2016. The status of domestic water demand: supply deficit in the Kathmandu Valley, Nepal. Water 8 (5), 196.
USGS, 2015. The Shuttle Radar Topography Mission (SRTM) Collection User Guide.
Viviroli, D., Dürr, H.H., Messerli, B., Meybeck, M., Weingartner, R., 2007. Mountains of the world, water towers for humanity: typology, mapping, and global significance. Water Resour. Res. 43 (7), 1–13.
Vuille, M., et al., 2008. Climate change and tropical Andean glaciers: past, present and future. Earth Sci. Rev. 89 (3–4), 79–96.
Wahrhaftig, C., Cox, A., 1959. Rock glaciers in the Alaska range. Geol. Soc. Am. Bull. 70 (4), 383–436.
Wang, X., et al., 2016. Mapping and inventorying active rock glaciers in the Northern Tien Shan (China) using satellite SAR interferometry. Cryosphere Discuss. 2016, 1–36.
Watson, C.S., Carrivick, J., Quincey, D., 2015. An improved method to represent DEM uncertainty in glacial lake outburst flood propagation using stochastic simulations. J. Hydrol. 529 (Part 3), 1373–1389.
Williams, M.W., Knauf, M., Caine, N., Liu, F., Verplanck, P.L., 2006. Geochemistry and source waters of rock glacier outflow, Colorado Front Range. Permafr. Periglac. Process. 17 (1), 13–33.
Winkler, G., Pauritsch, M., Wagner, T., Kellerer-Pirklbauer, A., 2016a. Reliktische Blockgletscher als Grundwasserspeicher in alpinen Einzugsgebieten der Niederen Tauern. Berichte der Wasserwirtschaftlichen Planung Steiermark. Bandolier 87, 134 (in German).
Winkler, G., et al., 2016b. Identification and assessment of groundwater flow and storage components of the relict Schoneben Rock Glacier, Niedere Tauern Range, Eastern Alps (Austria). Hydrogeol. J. 24 (4), 937–953.
Yu, L., Gong, P., 2012. Google Earth as a virtual globe tool for Earth science applications at the global scale: progress and perspectives. Int. J. Remote Sens. 33 (12), 3966–3986.